DESIGN OF AN EXPERIMENTAL SETUP FOR TWO PHASE FLOW STUDIES IN NEAR HORIZONTAL UPWARD AND DOWNWARD PIPE ORIENTATIONS

By

EDGAR IGNACIO LARES BARBOZA

Bachelor of Science in Mechanical Engineering

Universidad del Zulia

Maracaibo, Venezuela

2009

Submitted to the Faculty of the
Graduate College of the
Oklahoma State University
in partial fulfillment of
the requirements for
the Degree of
MASTER OF SCIENCE
July, 2014

DESIGN OF AN EXPERIMENTAL SETUP FOR TWO PHASE FLOW STUDIES IN NEAR HORIZONTAL UPWARD AND DOWNWARD PIPE ORIENTATIONS

Thesis Approved:

Dr. Afshin J. Ghajar

Thesis Adviser

Dr. Khaled Sallam

Dr. A. J. Johannes

ACKNOLEDGEMENTS

I would like to express my sincere gratitude to my advisor Dr. Afshin J. Ghajar for all his support, guidance and consistent encouragement throughout my graduate study at Oklahoma State University. I would also like to express my appreciation to Dr. Khaled A. Sallam and Dr. A.J. Johannes for investing their valuable time to serve as committee members. I would like to thank all the colleagues who worked with me on this research, Swanand Bhagwat, Kalapatapu Srinaga Bharath Chandra, Tabassum Aziz Hossainy, Adekunle Oyewole. Special thanks to Adekunle Oyewole, Kalapatapu Srinaga Bharath Chandra and Tabassum Aziz for their continuous support, valuable advises and friendship.

My ultimate gratitude extends to my mother for all her support and encouragement, which have inspired me to work hard towards achieving my professional goals. Her love and blessings made it possible for me to go this far to grow as a person and as a professional engineer. I would also like to thank my brothers Diego Alberto Lares Barboza and Tomas Eduardo Lares Barboza, as well as my love Gisselle Maria Russian Urdaneta for all their support and inspiration.

"Acknowledgements reflect the views of the author and are not endorsed by committee members or Oklahoma State University"

Name: LARES BARBOZA, EDGAR IGNACIO

Date of Degree: JULY, 2014

Title of Study: DESIGN OF AN EXPERIMENTAL SETUP FOR TWO PHASE FLOW STUDIES IN NEAR HORIZONTAL UPWARD AND DOWNWARD PIPE ORIENTATIONS

Major Field: MECHANICAL ENGINEERING

Abstract: Two phase flow has numerous industrial applications and some of them are related to transport of fluids, such as natural gas transportation. In which the pipe is not always horizontal and tends to be at upward or downward orientations. In the past decades, investigations have been conducted mostly in horizontal, vertical and upward flow. However, very little information is available for downward flows. An experimental setup was designed and constructed for the purpose of investigating heat transfer, pressure drop and void fraction for upward and downward flow. This investigation focused on two phase flow void fraction and flow visualization on a 25.4 mm diameter pipe for different downward flow inclinations. A flow map was developed for -5^{o}, -10^{o} and -20^{o} degrees of inclination describing the different flow pattern transition lines. A flow map comparison was performed between the flow map obtained in the present study and the one developed by Ghajar & Bhagwat (2014) for 12.7 mm pipe diameter pipe. The pipe diameter effect in the transition lines between different flow regimes was analyzed. An evaluation was conducted on thirteen well-known void fraction correlations available in the literature, where Gomez et al. (2000) showed the best performance overall. Also, a comparison of void fraction correlations performance for different pipe diameters was studied by comparing the results obtained in the present study with the results shown by Oyewole (2013) for a 12.7 mm pipe diameter. It was found that even though the pipe diameter is different, the performance of the selected void fraction correlations was analogous.

TABLE OF CONTENTS

LIST OF TABLES

Table Page

LIST OF FIGURES

Figure Page

NOMENCLATURE

A	Cross sectional area, m^2
C_o	Distribution parameter
D	Pipe diameter, m
f	Friction factor
Fr	Froude number
g	Acceleration due to gravity, $m\ s^{-2}$
G	Flux, $kg\ s^{-1}\ m^{-2}$
L	Length, m
La	Laplace number
$\dot{m}$	Mass flow rate, $kg\ s^{-1}$
P	Pressure, $kg\ m^{-1}\ s^{-2}$
Q	Volumetric flow rate
Re	Reynolds number
S	Perimeter over which stress acts, m
Sr	Slip ratio
U	Velocity, $m\ s^{-1}$

V Volume, m^3

w Uncertainty

We Weber number

x Thermodynamic quality

Greek symbols

α Void fraction

α_H Homogenous void fraction

ß Gas volumetric flow fraction

δ Liquid film thickness, m

ϵ Surface roughness

ε Liquid holdup

γ Liquid film height for flat stratified interface, m. Equation (4.5)

λ Input liquid content

μ Dynamic viscosity, kg m^{-1} s^{-1}

υ Kinematic viscosity, m^2 s^{-1}

ρ Density, kg m^{-3}

σ Surface Tension, kg m^{-1} s^{-2}

τ Shear stress, kg m^{-1} s^{-2}

θ Inclination angle, ^{o}

Subscripts

cr Critical

cs Cross sectional

dy Dynamic

h Hydraulic

g Gas

gm Drift

i	Interfacial
l	Liquid
m	Mixture
s	Superficial
sg	Superficial gas
sl	Superficial liquid
sys	System
tp	Two phase

Superscript

*	Dimensionless

CHAPTER I

INTRODUCTION

Two phase flow is defined as the simultaneous movement of two differing phases in a flow stream. There are different forms and combinations in which two phase flow can occur. For example when liquid and gas are flowing together, the flow could be constituted by gas bubbles flowing within the liquid. Another type of two phase flow is when gas and solid phases are present in the flow, like in the case of sand blasting or combustion of pulverized coal.

Two phase flow can be obtained when a single component of the same chemical composition is changing from one phase to another. For example: boiling or condensation. In contrast, two phase flow can also be found when it is composed by two differing chemical substances like in the case air and water in a mixed flow. There are several applications regarding two phase flow, and it is commonly found in industries such as: oil and gas, and power generation.

Some of the measurable properties on two phase flow are: void fraction, pressure drop, axial and surface temperatures, and mass flow rates, among others. Moreover, dimensionless parameters

are considered, such as: Reynolds, Prandtl, Webber, Froud, Nusselt numbers and are often used to explain the physics of an observed phenomenon. For example in the case of flow reversal which can be observed in upward flows, Oyewole (2013) utilized dimensionless numbers such as: Froude number, Reynolds number and Webber number to explain the phenomenon.

Void fraction in general is defined as the ratio of a geometric quantity (area or volume) of the gas phase and the total (area or volume) of the mixture. This gives valuable information of the two phase flow, and consequently it comes in handy when calculating different parameters that describe the nature of the mixed flow. For example, void fraction is used for the calculation of the superficial velocities, viscosity and density of the two phase flow. Also, void fraction is an empirical property and it can be only obtained experimentally, this is the reason some experiments on void fraction have been conducted in the past. Investigators have considered specific experimental conditions in order to acquire data with the purpose of obtaining correlations that would predict void fraction. Other investigators like the case of Bhagwat & Ghajar (2013) have used their experimental data in combination with other investigator's data so as to have a broader scope of information to work with. Therefore, their produced correlations would be versatile and with greater applicability. Void fraction is one of the parameters analyzed in this study, due to its importance in describing the two phase flow physics and phenomenon associated with this complex topic.

Furthermore, another important aspect of two phase flow is flow patterns. Oyewole (2013) mentioned that "flow patterns occurred when gas and liquid are simultaneously flowing in a pipe, spatial arrangement of liquid and gas occur due to difference in fluid properties (density and viscosity)". In comparison with single phase flow, where there is just one phase of liquid or gas, two phase flow handles different types of flow patterns. At the interface between liquid and gas, interface shear stresses are present, and are an important factor on the formation of different flow patterns. Also, small changes in mass flow rates, generate different flow patterns such as:

(stratified) when liquid is separated from the gas phase, (bubbly) when gas bubbles are flowing within the liquid flow phase, (slug flow) when air bubbles collide until forming a big gas pocket that travels through the pipe and which is separated by a slug of liquid, (annular) when gas is flowing only at the core and liquid is flowing at the wall. There are many other sub-types of flow patterns, due to different transition boundaries that exist between one flow pattern and the other. Frequently these transition lines are subjective and different authors name these regions differently.

The two phase flow parameters are also affected by the change in the inclination angle of the pipe as well as the direction of the flow (upward or downward flow). When these geometry parameters are modified, physical properties of two phase flow also change. Thus, different flow patterns are created and changes in void fraction in the system are observed.

In the past, studies have been conducted in the area of two phase flow. The majority of the applicability of the correlations for void fraction, heat transfer and pressure drop by different authors is restricted to small sets of experimental data. In a study made by Woldesemayat & Ghajar (2007), 68 correlations from the literature were studied. It was observed that the range in which these correlations were applicable was found to be limited, showing that some of the correlations showed stupendous results under certain conditions while others exhibited poor performances in other regions.

Most of the experimental data that is found in the literature is mainly focused on horizontal or vertical orientations, and limited studies were found for different inclinations. From the few studies that were conducted on inclined pipes, upward cases exceed downward flows. This leaves downward flows with almost no information available in the literature.

Research in the area of two phase flow has been conducted at Oklahoma State University, Two Phase Laboratory is well equipped and efforts have been made towards the further enhancement

of knowledge in this important subject. In order to collect the data necessary for developing correlations, an experimental apparatus was developed by Clement Tang, former Ph.D. student, for systematic heat transfer data collection system in horizontal and upward inclined positions (up to 7°) in a 25.4 mm pipe. This experimental setup was capable of producing a variety of flow patterns and included two transparent flow visualization sections for the purposes of detailed flow pattern visualization and flow pattern mapping. The general heat transfer correlation developed through the use of this experimental apparatus has been published in numerous papers and is published most recently in Ghajar & Tang (2007). This experimental setup had few limitations, such as the range of inclination (only up to 7° in upward flow) and the inability to take void fraction measurements.

For this reason an experimental setup was constructed by Cook (2008). This one was a 12.7 mm pipe experimental setup with a range of inclination of +/- 90°. Also it incorporated the void fraction measurement capability. In this experimental setup studies have been conducted on heat transfer, void fraction and pressure drop for different inclinations for the past several years.

However, in order to improve the accurateness and to expand the applicability of the correlations generated in these experimental facilities, it was necessary to account for the pipe diameter as a variable that could affect the performance of the correlations. The experimental setup developed by Tang (2011) was designed only for upward flow and up to 7° of inclination, which restricts the possibility of comparing the data from both experimental setups.

In order to introduce the pipe diameter effect and further extend the capabilities of the correlations, a new experimental apparatus was developed. The new 25.4 mm experimental setup has two sections. The first section serves for measurement of void fraction and pressure drop as well as for flow visualization on a smooth transparent pipe. The second section is for measuring pressure drop and heat transfer on a rough stainless steel pipe. A hydraulic mechanism was

designed so as to give the experimental setup an inclination capability of +/- 20°, as well as the setting option for upward or downward flows. Added to this, quick solenoid valves were selected and installed for the purpose of measuring void fraction.

In addition to the design and construction of a new 25.4 mm experimental apparatus, a study on void fraction was performed. The purpose of this study was to evaluate the influence of the pipe diameter as a variable that could affect the flow patterns and therefore the void fraction. This influence was assessed by comparing the previous studies made by Oyewale (2013) in the 12.7 mm experimental setup of the Oklahoma State University Two Phase Flow laboratory.

The following research questions were examined:

- What is the flow pattern map for downward flow in a 25.4 mm diameter pipe?
- What is the effect of flow patterns on void fraction for downward flow in a 25.4 mm diameter pipe?
- What is the performance of well-known void fraction correlations from the literature in the case of downward flow for a 25.4 mm pipe?
- What is the effect of pipe diameter as a variable that could affect the performance of void fraction correlations?

The present study is divided into four chapters. Literature review is developed in Chapter II and it is divided in to three sections, flow patterns, flow maps and void fraction correlations. Thirteen correlations were selected for the purpose of this study and details are shown in Chapter II. Chapter III focuses on the new designed experimental setup presenting the description of each section, calibration of the instrumentation, validation, uncertainty calculations and experimental procedures. In Chapter IV results were presented. These results showed the different flow patterns observed as well as the flow map created for three different downward inclinations (-5^o, -10^o, -20^o). The effect of downward pipe orientation on flow patterns and transition boundaries on

the flow map were analyzed in Chapter IV. The performance of selected void fraction correlations was evaluated in order to come up with the best performing correlation in downward flow. The final part of Chapter IV focuses on the pipe diameter influence on the performance of void fraction correlations. Chapter V draws conclusions and recommendations from the results obtained in Chapters III and IV.

CHAPTER II

LITERATURE REVIEW

For decades, several investigators have concentrated their studies in two phase flow due to the extensive number of applications found in the industry. This chapter focuses on investigations related to: flow patterns, flow mapping and void fraction, therefore the chapter is divided in three sections.

The first part discusses the flow patterns observed in inclined pipes for near horizontal orientations, as well as showing details about their experimental setups and methods used for flow visualization. The second part discusses information about flow maps developed by several investigators for different orientations. In the case of the present study, flow visualization was performed and more than 300 data points were observed so as to create flow maps that characterized the newly designed experimental setup. For this reason, previous investigations on flow patterns and flow mapping were analyzed and are well described in this literature review chapter.

Lastly, the third section discusses some of the most used void fraction correlations in the literature. These same correlations were evaluated and details about their performance can be found in Chapter IV.

2.1 FLOW PATTERNS

Beggs & Brill (1973) led two phase flow studies in inclined pipes over the entire pipe orientation range from $+90^{o}$ to -90^{o} in 25.4 and 38.1 mm pipe diameters. They categorized the flow patterns as follows: segregated flow, intermittent flow and distributed flow. Segregated flow consists of stratified flow, wavy flow and annular flow. Intermittent flow is made of plug and slug flow while distributed flow consists of bubble flow and mist flow.

Spedding & Nguyen (1980) performed research studies on air-water two phase flows in a 45.5 mm pipe diameter for vertical downward and upward flows. Flow visualization was obtained by performing observations in a clear transparent pipe, measuring pressure fluctuation at the wall and by photography using x-rays or fluorescent light. The flow patterns observed were: stratified flow, bubble-slug flow, droplet flow and mixed flow. Stratified flow was sub divided into straight stratified, stratified plus ripple, stratified plus roll and stratified plus inertial wave. They described that by keeping the liquid flow rate constant and increasing the gas phase flow rate in horizontal pipe orientation, straight stratified flow progressed into stratified plus ripple waves and then to stratified plus roll waves. An increase in gas flow rate led to droplets being torn from the liquid interface, the straight stratified flow was observed to completely disappear under these conditions and the flow pattern was termed stratified flow plus inertial waves. They also stated that straight stratified flow was difficult to obtain in upward inclined pipe orientation. For downward inclined pipe orientation, straight stratified flow was observed to persist over a very wide range of liquid flow rates while bubble flow was difficult to achieve.

Barnea et al. (1982) led experimental studies on flow patterns in downward inclined two phase flow. The experimental apparatus used consisted of two transparent plexi-glass 10 m long pipes with internal diameters of 25.5 mm and 51 mm. The apparatus has the capacity of variable inclination from horizontal to vertical. They carried out visual observation and also employed an oscilloscope display which uses electro conductivity probes to determine the flow patterns. The flow patterns observed were: stratified, slug, bubbly and annular flow. They categorized stratified flow into two types based on the nature of the interface, smooth stratified flow and wavy stratified flow.

Barnea et al. (1985) studied transition of flow patterns for upward flow, utilizing air-water as the working fluid. Eight flow patterns were observed in the horizontal pipe and were categorized into four types. The categories of flow patterns observed were: stratified, intermittent, annular and dispersed bubble.

Mukherjee & Brill (1985) performed experimental two phase flow studies in a 50.8 mm pipe for various pipe orientations in both upward and downward inclinations. The flow patterns observed were: slug, bubbly, stratified and annular. They observed at downward pipe orientations, that bubble rise velocity is always counter-current to the general flow direction which leads to shear of large bubbles into smaller bubbles. Stratified flow was observed in horizontal and downward inclined pipe orientations. They reported that a velocity gradient exist across the liquid film in downward inclined pipe orientation for stratified flow, this velocity gradient was observed to increase with further shift in pipe orientations in the downward direction. Annular flow was observed in both upward and downward inclined pipe orientations which they described as the gas phase being continuous along the pipe core. They also described the nature of the continuous gas phase (either concentric or not) in annular flow as dependent on pipe orientation in both upward and downward flows.

Kokal & Stanislav (1989) performed experimental two phase flow studies and used the combination of air and oil, with a test section of 25 m long pipe and different pipe diameters of 25.8 mm, 51.2 mm and 76.3 mm. Added to that, the experimental apparatus served for an inclination range of $\pm 10^{o}$ from horizontal. Flow patterns were determined using volume sensor traces. Flow patterns were categorized into 3 major regions: gas dominated flows, liquid dominated flows and intermittent flow. For the gas dominated flows the flow patterns observed were: stratified flow, annular flow, intermittent flow, elongated bubble flow, elongated bubble with dispersed bubble flow and slug flow. For the case of the liquid dominated flows, the flow patterns were divided as: dispersed bubble flow and dispersed froth flow. Lastly, for the intermittent flow a combination of liquid slugs and large bubbles were described.

Dezhang & Ning (1992) performed research on flow pattern and heat transfer of boiling two phase flow in upward and downward inclined pipes. Flow visualization was observed at the following inclinations: 0^{o}, $\pm 30^{o}$, $\pm 60^{o}$ and $\pm 90^{o}$. Various flow patterns were analyzed based on heat flux and pipe orientation. The major flow patterns were categorized as: slug, annular, wavy and saturated bubble flows, also slug/annular and bubble/slug flows were included.

Spedding et al. (1999) performed research studies on co-current two phase flows in inclined pipe. Flow visualization was completed in an 11.28 m long and 50.8 mm internal diameter pipe with a range of inclination of $\pm 5^{o}$ from horizontal. The working fluids utilized were air and water as a two phase flow mixture. The flow patterns observed were: stratified, annular, slug and bubble flows.

Tshuva et al. (1999) performed research studies on two phase flow in parallel inclined pipes for 24 mm diameter pipe with an inclination angle range of 0^{o} to 90^{o}. Quick closing valves were used for the measurement of void fraction and they also assessed the symmetry of flow in the pipe. Flow patterns were divided into symmetric and asymmetric flow. They observed that in the low

liquid and gas flow rate region and at low pipe inclinations, flow starts symmetric and progresses into asymmetric flow as pipe inclination increased.

Oddie et al. (2003) performed research studies on two phase flow in a pipe with diameter of 150 mm and length of 11 m, over inclination angles of $+90^o$ to -2^o with respect to horizontal. Different fluid combinations were used. The flow patterns observed were: bubble, churn, stratified, slug, elongated-bubble and stratified wavy flows. They observed bubble flow in vertical and 5^o deviation from vertical orientation. At 45^o, a combination of slug flow, churn flow and elongated–bubble flow was observed where churn flow was the dominant flow pattern. It was reported that as pipe inclination shifted to 70^o from vertical, slug and elongated-bubble flow were the only flow patterns observed and at 90^o and 92^o from vertical, stratified and stratified wavy flows were observed at constant flow rates.

Tang (2011) performed experimental two phase flow studies on horizontal and slightly inclined pipe having a diameter of 27.9 mm. Flow visualization was attained over inclination angles of $+0^o$, $+2^o$, $+5^o$ and $+7^o$. The flow patterns observed for horizontal pipe orientation were somewhat different from those observed in the inclined pipe orientations. The flow patterns observed in this study were: stratified, slug, plug, wavy and annular flows. Slug/wavy flow, slug/bubbly flow and wavy/annular flow were observed as transition flow patterns as well. He observed that stratified flow at 0^o was replaced by slug flow at small inclination angle of 2^o and there was an increase in wave height and splashing for each flow pattern as pipe orientation increased beyond 2^o through 5^o then to 7^o.

In sum, similar types of flow patterns were observed by different investigators in the case of near horizontal pipe orientations. The most frequently observed flow patterns for downward flow were: slug, stratified, annular and intermittent flows. These flow patterns were observed in the present study and further information about the flow visualization can be found in Chapter IV.

2.2 FLOW MAPS

Hewitt & Wallis (1963) led experimental studies on two phase flow and introduced a flow pattern map for the case of vertical upward flow, shown in Figure 1. The vertical axis represents the superficial gas momentum flux and the horizontal axis represents the superficial liquid momentum flux.

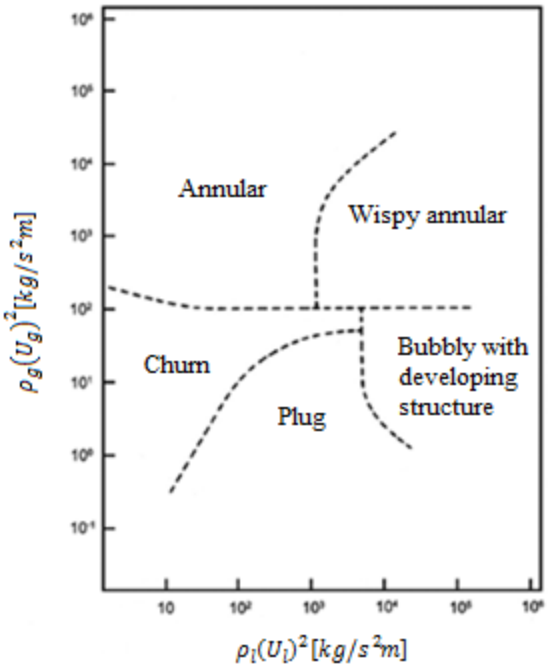

Figure 1 Flow map for vertical upward flow by Hewitt and Roberts (1969)

Mandhane et al. (1974) conducted studies on horizontal two phase flow on 25 mm diameter pipe at 25^{o} C and 1bar. Figure 2 demonstrates the flow map developed where solid lines and points are experimental observations of the transition between flow patterns. The hatched regions represent theoretical predictions.

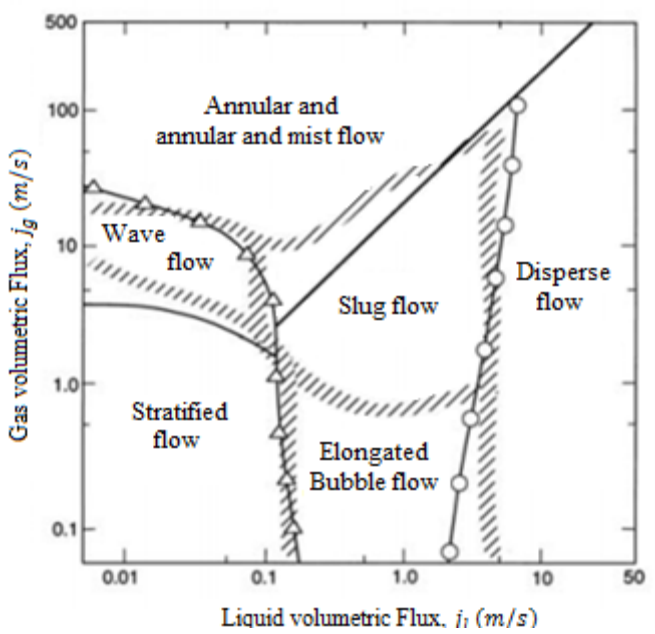

Figure 2 Horizontal flow pattern map developed by Mandhane et al. (1974)

Spedding & Nguyen (1980) led studies on flow regime maps for two phase flow in different pipe orientations. They reported that the main error from flow map comparison was due to inaccurate drawings of the transition lines between flow patterns and difference in flow parameter used to develop the flow maps to be compared. Their horizontal flow map is shown in Figure 3.

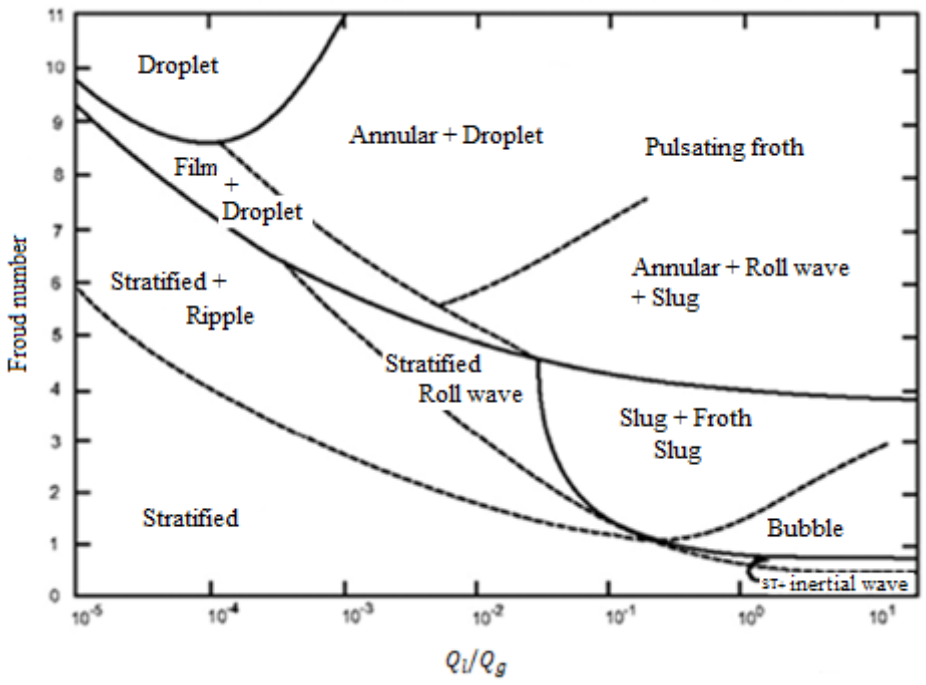

Figure 3 Flow map for horizontal flow by Spedding & Nguyen (1980)

Spedding & Spence (1993) examined flow regimes in two phase gas liquid flow by performing co-current experiments in a 93.5 mm diameter horizontal pipe. Visual observations were carried out and pressure fluctuations were measured to determine flow pattern in the two phase flow. Preexisting maps from different investigators were analyzed and compared with their investigation. They reported that the previous regime maps and theories did not satisfactorily predict their observation as consequence of some differences in flow parameters adopted.

In sum, the procedure for developing flow maps is subjective to the investigator, and it often depends on factors such as: the experimental setup, pipe orientations and the parameters considered. In the present study flow maps were developed with information obtained by flow visualization, as discussed in Chapter IV.

2.3 VOID FRACTION

Void fraction is an essential parameter in two phase flow. In general is defined as the ratio of a geometric quantity (area or volume) of the gas phase and the total (area or volume) mixture. Depending on the geometric parameter, the void fraction can be named as local void fraction, cross sectional void fraction and volumetric void fraction. The local and cross sectional void fraction suggests the value of void fraction at a specific point and the distribution of the gas phase in the entire cross sectional area. The cross sectional void fraction is defined as:

$$\alpha = \frac{A_g}{A_g + A_l}$$

where, A_g is the cross sectional area occupied by the gas phase and A_l is the cross sectional area of the liquid.

Another definition is the volumetric void fraction, which is defined in terms of volumes of gas and liquid phases as follows:

$$\alpha = \frac{V_g}{V_g + V_l}$$

where, V_g is the volume occupied by the gas. Similarly, V_l is the liquid volume in the section. This type of void fraction is often used in experimental setups of relatively small diameters. A set of quick closing valve is used to trap the volume of the mixture and thus calculate this ratio.

DRIFT FLUX MODEL

Wallis (1969) defined the drift flux model as a separated flow model based on relative velocity between the phases. Drift flux model can be used to analyze flow patterns such as slug flow, stratified flow, annular flow, bubble flow and mixed flow patterns for both steady and unsteady two phase flow. For gravity dominated flows, Wallis (1969) explained that the drift flux model

analyzes the flow regimes appropriately by balancing out the pressure gradient and the forces between the components. The first drift flux model was proposed by Zubar & Findlay (1965), which was a one dimensional formulation where, U_{sg} is superficial velocity of gas phase, U_m is superficial velocity of the two phase mixture ($U_{sg} + U_{sl}$), $C_o$is distribution parameter, U_{gm} is the drift velocity. The drift velocity can either be positive or negative in value depending on the direction of the gas phase relative to the two phase mixture. Assuming that fluid properties are constant across pipe cross section, cross sectional flow averaging is applied to the drift flux model and is shown as

$$\langle \alpha \rangle = \frac{\langle U_{sg} \rangle}{C_o \langle U_m \rangle \pm U_{gm}}$$

By definition the average value of any variable b is gives as,

$$\langle b \rangle = \frac{1}{A} \int b dA$$

The distribution parameter is defined as the concentration of the gas phase across pipe cross section and as explained by Wallis (1969), it is also used as a correction to the one dimensional flow theory which does not account for concentration across pipe cross section. The mathematical representation of distribution parameter is given as

$$C_o = \frac{\langle \alpha U_m \rangle}{\langle \alpha \rangle \langle U_m \rangle}$$

This term was defined by Wallis (1969) as an expression for the distribution parameter, which is the ratio of the average of the product of mixture superficial velocity and concentration to the product of the averages can be used to obtain near unity parameters in two component flows.

The other term defined by Wallis (1969) was the drift velocity, which is the ratio of the averaged product of concentration and the difference between the component velocity and the mixture

velocity to the cross sectional averaged concentration. The mathematical representation of drift velocity is given as:

$$U_{gm} = \frac{\langle \alpha (U_g - U_m) \rangle}{\langle \alpha \rangle}$$

VOID FRACTION CORRELATIONS

Lockhart & Martinelli (1949) proposed one of the first void fraction correlations for horizontal pipe orientation, the expression was given as:

$$\alpha = \left[1 + 0.28(1 - x/x)^{0.64} \left(\rho_g/\rho_l\right)^{0.36} \left(\mu_l/\mu_g\right)^{0.07}\right]^{-1}$$

Nicklin et al. (1962) suggested a void fraction expression based on drift model, which was focused on the bubble velocity in a slug flow for air-water fluid combination in a 0.025 m ID pipe. The expression can be written in the following form:

$$\alpha = \frac{U_{sg}}{C_o U_m + U_{gm}}$$

$$where\ C_o = 1.2\ and\ U_{gm} = 0.35\sqrt{gD}$$

Guzhov et al. (1967) correlation for predicting void fraction was reported by Woldesemayat & Ghajar (2007). This correlation was developed for slug and stratified flow, in pipe with orientation range of ±9^o from horizontal. Their correlation is given as:

$$\alpha = 0.81\beta\left(1 - \exp(-2.2\sqrt{Fr}\right),\ \beta = \frac{U_{sg}}{U_{sl}+U_{sg}}\ and\ Fr = \frac{\left(U_{sl}+U_{sg}\right)^2}{gD}$$

Smith (1969) established a correlation for two phase flow annular flow. It is based on the slip ratio which assumes an equal velocity head model for the liquid phase as well as a homogenous

mixture so as to predict the void fraction. This correlation can also be applicable for inclined pipe orientations, and is given as follows:

$$\alpha = \left(1 + \frac{\rho_g}{\rho_l}\left(\frac{(1-x)}{x}\right)\left[0.4 + 0.6\left(\frac{\rho_l/\rho_g + 0.4(1/x - 1)}{1 + 0.4(1/x - 1)}\right)^{0.5}\right]\right)^{-1}$$

Rouhani & Axelsson (1970) conducted studies on two phase flow and reported a void fraction correlation for upward two phase flow utilizing the drift flux model, as shown:

$$\alpha = \frac{U_{sg}}{C_o U_m + U_{gm}}$$

Experimental data was obtained using steam water as the working fluid. The drift velocity term was expressed as a function of the densities, surface tension at the interface and the quality, as shown below:

$$U_{gm} = 1.18\left(g\sigma\frac{(\rho_l - \rho_g)}{{\rho_l}^2}\right)^{0.25}$$

The distribution parameter in this correlation is expressed as:

$$C_o = 1 + 0.2(1-x)\ for\ \alpha > 0.25$$

$$C_o = 1 + 0.2(1-x)\left(\frac{gD{\rho_l}^2}{G^2}\right)^{0.25}\ for\ \alpha > 0.25$$

Bonnecaze et al. (1971) performed investigations on two phase slug flow for an inclination of ± 10 degrees from horizontal. They proposed a correlation which was based on the drift flux concept. The correlation was developed to predict void fraction in a gas- oil two phase mixture at different inclinations of the flow. They evaluated the effect of the inclination on the drift velocity

and determined that the drift velocity magnitude initially increases with decreasing inclination from vertical orientation and subsequently it decreases. The correlation proposed is given below:

$$\alpha = 1 - \frac{1-\beta}{1.2 + 0.35\left(1 - {}^{\rho_g}/_{\rho_l}\right)/\delta\sqrt{Fr}}$$

$where, \delta = -1$ in the case of downward flow.

Sun et al. (1981) suggested a void fraction expression centered on drift flux concept. It was based on vertical upward flow. The pressure term was introduced in the distribution parameter. The correlation is shown below:

$$\alpha = \frac{U_{sg}}{C_o U_m + U_{gm}}$$

where, $C_o = \left[0.82 + 0.18\left(P_{Sys}/P_{cr}\right)\right]^{-1}$ and $U_{gm} = 1.41\left(g\sigma\frac{\rho_l - \rho_g}{\rho_l{}^2}\right)^{0.25}$

Morooka et al. (1989) led void fraction studies on vertical 4 x 4 rod bundles for steam-water two phase flows using advanced X-ray CT scanner. Pressure, quality and mass flux were parameters considered to evaluate the void fraction. Utilizing measured data, they developed a drift flux model to predict void fraction in vertical pipe for upward flows, as show below:

$$\alpha = \frac{U_{sg}}{1.08U_m + 0.45}$$

Gomez et al. (2000) adapted the drift velocity expression suggested by Hasan & Kabir (1988) in order to account for the void fraction in bubbly flow at different upward orientations from 0 to +90 degrees. The correlation proposed by them is shown below:

$$\frac{U_{sg}}{\alpha} = \left(C_o U_M + U_{gm} sin\theta (1-\alpha)^{0.5}\right)$$

where, and $C_o = 1.15$ and U_{gm} is the drift velocity defined by Haramathy (1960) as shown:

$$U_{gm} = 1.53\left(\frac{g\sigma\Delta\rho}{{\rho_l}^2}\right)^{0.25}\sqrt{1-\alpha}sin\theta$$

Yashar et al. (2001) led experimental studies on two phase flow, utilizing refrigerants R134a and R410A so as to determine void fraction for the cases of condensation and evaporation processes in horizontal tubes. Tubes had diameters of 7.3 mm and 8.9 mm with the axial and 18 degree helix which were 1.2 m long were used for experimentation. Condensation experiments were conducted in the 8.9 mm diameter tube while the evaporation experiment was carried out for both 7.3 mm and 8.9 mm diameter tubes. Quick closing valves were used in order to acquire void fraction measurements. Collecting sufficient experimental data a correlation was developed to predict void fraction, which is presented below:

$$\alpha = \left[1 + \sqrt{\frac{(1-x)gD{\rho_l}^2}{G^2x^3} + \left(\frac{1-x}{x}\right)^{0.9}\left(\frac{\rho_g}{\rho_l}\right)^{0.5}\left(\frac{\mu_l}{\mu_g}\right)^{0.1}}\right]^{-0.321}$$

Woldesemayat & Ghajar (2007) studied void fraction data for different pipe inclinations from 0 to +90 degrees. They worked on the correlation proposed by Dix (1971) and modified the expression. They included terms to account for various pipe inclinations and fluid properties. This correlation is based on the drift flux model:

$$\alpha = \frac{U_{sg}}{C_o U_m + U_{gm}}$$

And the distribution parameter was maintained as proposed byDix (1971). However, the drift velocity was modified and is given as follows:

$$U_{gm} = 2.9(1.22 + 1.22sin\theta)^{(P_{Sys}/P_{cr})}\left[\frac{gD\sigma(1+cos\theta)(\rho_l - \rho_g)}{{\rho_l}^2}\right]^{0.25}$$

It is important to notice that the $C_o = 2.9$ and carries the unit of $m^{-0.25}$.

Cioncoloni & Thome (2012) performed two phase flow studies in annular flow and established a correlation based on void fraction data points, with the purpose of predicting void fraction. The total amount of void fraction data points used was 2673, which were collected from 29 sources. These data covered 8 different fluid combinations, such as: air-water, nitrogen-water, argon-water, steam-water, R410a, air-kerosene, air-alcohol and water plus air-alcohol. Also, for pipe diameters from 1.05 mm to 45.5 mm. Added to this, geometry was considered accounting for data points for both circular and non-circular geometry. They developed a correlation utilizing biochemical kinetics. This correlation is a function of vapor quality and gas to liquid density ratio, given as:

$$\alpha = {hx^n}/{(1 + (h-1)x^n)}$$

where, $h = -2.129 + 3.129\left({\rho_g}/{\rho_l}\right)^{-0.2186}$ and $n = 0.3487 + 0.6513\left({\rho_g}/{\rho_l}\right)^{0.515}$

Bhagwat & Ghajar (2013) performed extensive research in two phase flow. Utilizing the drift flux model, they developed a correlation independent of flow patterns. The pipe orientations considered were in the range of -90^o to +90^o. Also for different types of geometries, such as: circular, annular and rectangular. The pipe diameter range was 0.5 to 305 mm. Fluids viscosity considered were in the range of 0.0001 Pa.s to 0.6 Pa.s, system pressure of 0.1 MPa to 18.1 MPa and a range of Reynolds number of 10 to 5x10^6. This correlation has the ability to predict void fraction for different fluid combinations like: air-water, argon-water, natural gas-water, air-kerosene, air-glycerin, argon-acetone, argon-ethanol, argon-alcohol, refrigerants (R11, R12, R22, R134a, R114, R410A, R290 and R1234yf), steam-water and air-oil.

The correlation was tested and verified with 8255 data points collected from more than 60 sources and its performance was very consistent in terms of accuracy for the collected data. The correlation is shown as follows:

Drift flux model:

$$\alpha = \frac{U_{sg}}{C_o U_m + U_{gm}}$$

where, C_o is function of $C_{o,1}$, Re_{tp}, β and $\sqrt{f_{tp}}$ as follows:

$$C_o = \frac{2 - \left({\rho_g}/{\rho_l}\right)^2}{1 + \left({Re_{tp}}/{1000}\right)^2} + \frac{\left[\sqrt{\left(1 + \left({\rho_g}/{\rho_l}\right)^2 cos\theta\right)\Big/(1 + cos\theta)}^{\,1-\alpha}\right]^{2/5} + C_{o,1}}{1 + \left({Re_{tp}}/{1000}\right)^2}$$

$$C_{o,1} = \left(C_1 - C_1\sqrt{{\rho_g}/{\rho_l}}\right)\left((2.6 - \beta)\right) - \sqrt{f_{tp}}\,(1 - x)^{1.5}$$

$$Re_{tp} = \frac{(U_{sl} + U_{sg})\rho_l D_h}{\mu_l}, \beta = \frac{U_{sg}}{U_{sl} + U_{sg}}, \frac{1}{\sqrt{f_{tp}}} = -4.0 log_{10}\left(\frac{{\varepsilon}/{D_h}}{3.7} + \frac{1.256}{Re_{tp}\sqrt{f_{tp}}}\right)$$

And U_{gm} is presented as function of C_1, C_2, C_3 and C_4shown:

$$U_{gm} = (0.35 sin\theta + 0.45 cos\theta)\sqrt{\frac{g D_h(\rho_l - \rho_g)}{\rho_l}}(1 - \alpha)^{0.5} C_2 C_3 C_4$$

$$C_1 = 0.2, C_2 = \begin{cases} \left(\dfrac{0.434}{log_{10}\left({\mu_l}/{0.001}\right)}\right)^{0.15} & \left({\mu_l}/{0.001}\right) > 10 \\ 1 & \left({\mu_l}/{0.001}\right) \le 10 \end{cases}$$

$$C_3 = \begin{cases} \left({La}/{0.025}\right)^{0.9} & La < 0.025 \\ 1 & La \ge 0.025 \end{cases}, La = \sqrt{{\sigma}/{(g\Delta\rho)}}\Big/ D_h$$

$C_4 = -1\ (0^o > \ \theta \ \geq -50^o), Fr_{sg} \leq 0.1, otherwise\ C_4 = 1$

In sum, thirteen correlations were discussed in this literature review. These same correlations were studied in the present study and an evaluation was conducted on their performance considering different factors, for the case of downward pipe inclinations. The analysis and results are shown in Chapter IV.

CHAPTER III

EXPERIMENTAL SETUP AND PROCEDURES

The experimental setup was designed and constructed with the capability of measuring void fraction, heat transfer and pressure drop data. It is divided into two 25.4 mm pipe diameter sections: one is a (stainless steel) rough pipe and the other one is a (PVC) smooth pipe. Additionally, the setup was designed to have upward and downward flow configurations with an inclination range of +/- 20 degrees. In this chapter, the description of the experimental setup and its instruments is introduced.

3.1 DESCRIPTION OF THE EXPERIMENTAL SETUP

In this section, the different components of the experimental setup will be described. This setup is part of the Oklahoma State University two phase flow laboratory, where another experimental setup of 12.7 mm pipe diameter is similarly operating. In this laboratory, the general components are utilized by both setups. These general components are presented below as well as the main components of the new designed experimental setup.

3.1.1 FLOW LOOP DIAGRAM

A diagram of the flow loop is shown in Figure 4. A centrifugal pump is used to increase the pressure of the distilled water which is contained in a reservoir. On the other hand, a reciprocal compressor located outside the building is used to increase the pressure of air until the proper operational pressure is obtained. In order to control the desired air pressure a regulator is placed inside the laboratory.

Increasing temperatures are often observed on the working fluids, due to the frictional forces or high environmental temperatures. For these reasons, both systems (air and water) have heat exchangers so as to control the temperatures and assure a proper functioning of the experimental setup.

It can be observed that after the tee connection shown in Figure 4, air and water are mixed within the mixing section (static mixer). On Figure 5 (top view), the smooth and rough pipes are shown to the left and right respectively. The smooth pipeline (PVC) is used for the void fraction, flow visualization and pressure drop measurements. While the other section is used for measuring pressure drop and heat transfer in a rough pipe (stainless steel).

These two pipe lines are resting on top of an aluminum I-beam, which is supported by a pivoting mechanism, specially designed to obtain variable inclinations. As mentioned before, the operating range of the experimental setup is +/- 20 degrees. The I-beam is approximately 9.1 m (30ft) long and the inclination angles were measured with a contractor's angle measuring tool.

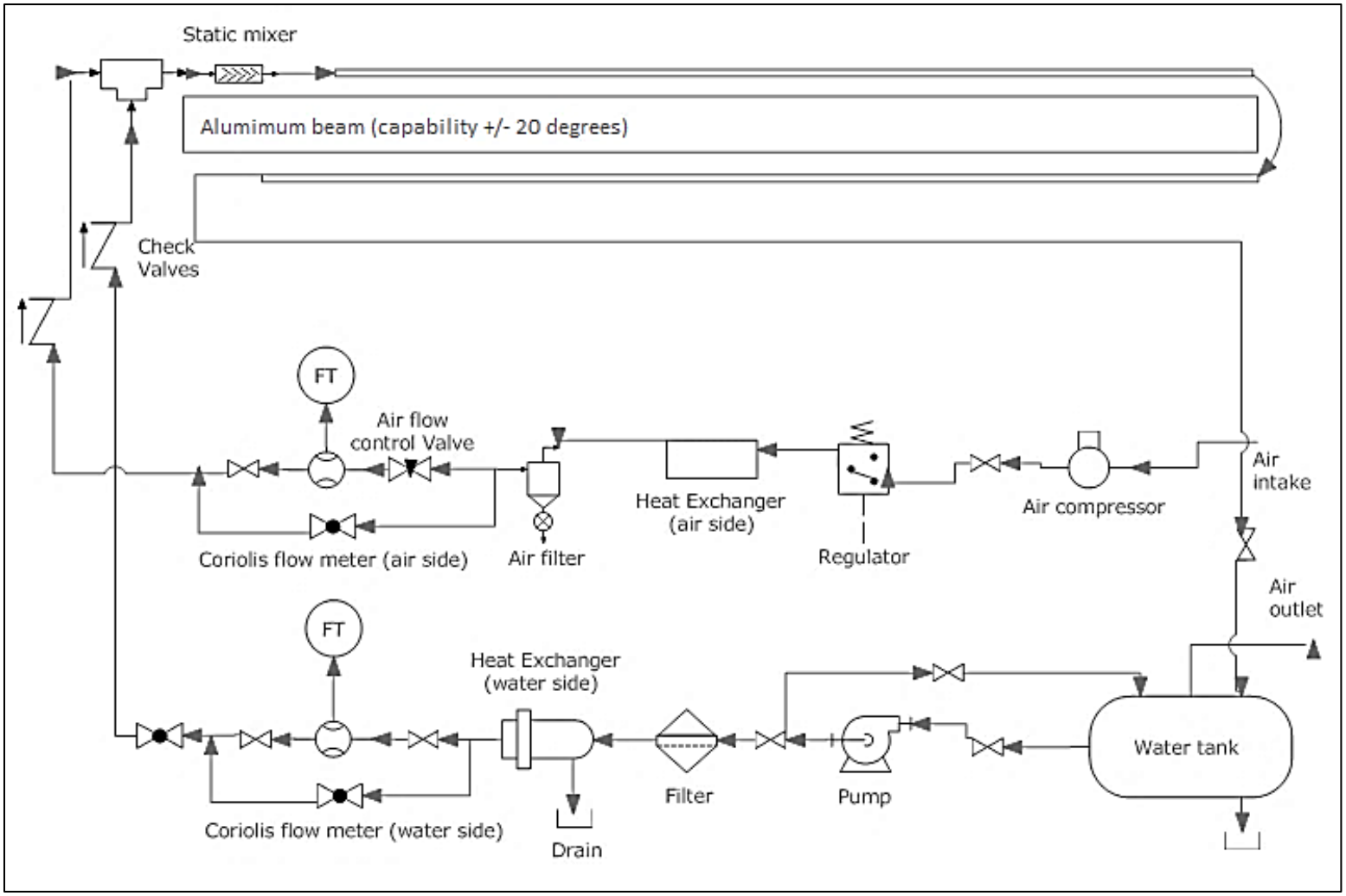

Figure 4 Flow loop of the experimental setup

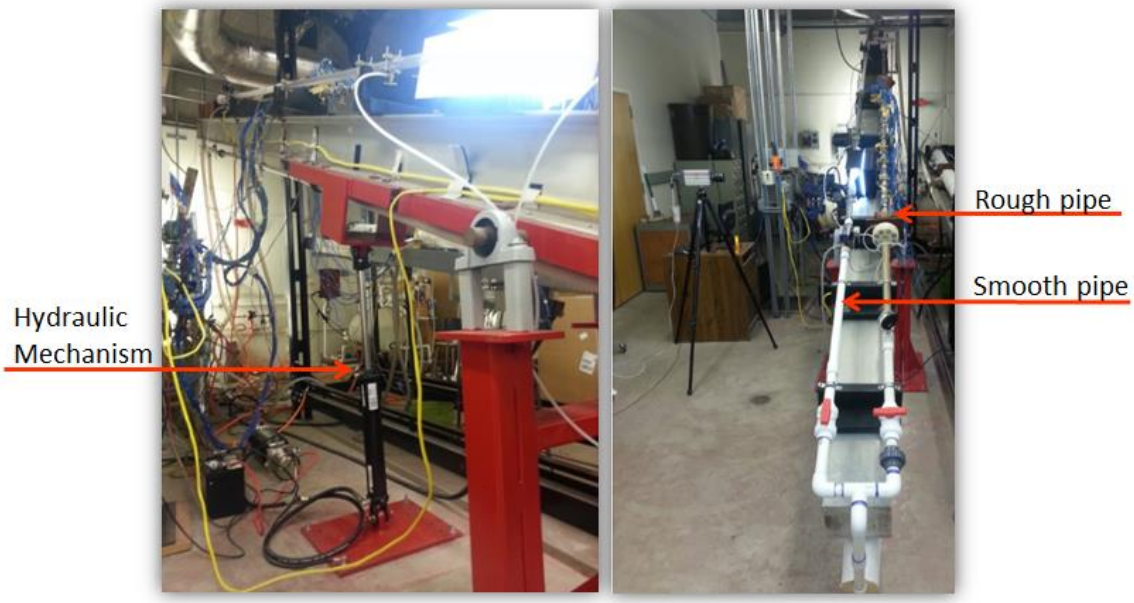

Figure 5 Experimental apparatus (lateral and top view)

3.1.2 SUPPLY OF WORKING FLUIDS

The working fluids used are: air and distilled water.

DISTILLED WATER TRANSPORT

The water is filtered by the reverse osmosis method at the Chemistry Department at Oklahoma State University. The distilled water was stored in a polyethylene cylindrical reservoir of a volume equal to 208-liter (55 gal). A centrifugal pump (Bell & Gosset Series 1535, size 3545 D10) is used to pump the distilled water from the reservoir and to run it through the setup until it comes back again to the water reservoir to close the loop. Once water runs through the setup, the maximum flow rate observed was 36.29 kg/min (80 lb/min).

The pumped distilled water is first filtered with an Aqua-Pure AP12T water filter, and then a heat exchanger (ITT standard model BCF 4063 one shell and two-tube pass heat exchanger) is used to remove heat that was added to the fluid during the process of running it through the experimental setup. The cooling fluid used in the heat exchanger is regular tap water at an average temperature of about 22 ^{o}C (71.6 ^{o}F). This cooling process is necessary so as to maintain a constant inlet temperature and therefore keep the same characteristics of the distilled water for each experimental run.

After the heat exchanger, the distilled water passes through a coriolis flow meter (Micro motion, model CMF125). The coriolis flow meter is connected to a digital transmitter (Digital field-mount, model RFT9739) that sends the flow information to the data acquisition system. After the coriolis flow meter, the distilled water then passes through a 25.4 mm regulator gate valve. This valve is utilized to control the flow of distilled water that is sent into the mixing section. Then after the regulator gate valve, the distilled water is transported to the air –water mixing section through a 25.4 mm hose, at the end of which a one way check valve is used to prevent any fluid return due to possible backup pressures at the entrance of the static mixer in the mixing section.

After the water and air mixture runs through the experimental setup it returns to the reservoir were air escapes via a curved vent.

AIR TRANSPORT

The airflow provided to the system is supplied by a compressor (Ingersoll-Rand T30, Model 2545). The maximum pressure that the compressor can achieve is 862 kPa (125 psi). The maximum flow rate is 1.2 kg/min (2.64 lb/min). The air is regulated by a 1/2 inch air regulator (Speedaire, Model 4ZM22). The air is then cooled by passing it through a serpentine made of copper which is submerged in a vessel where cooling water is supplied from the wall tap. The tap water used in this system is the same used for cooling of the distilled water, so as to ensure that both air and distilled water have the same inlet temperature. After this stage, the air enters into a 12.7 mm air filter (Speedaire, Model 4ZL49) with the purpose of removing moisture from the air before flow rates are measured.

Subsequently, the air is filtered and flows through a coriolis flow meter (Micro Motion, Model CMF100) which is connected to a digital transmitter (Digital Field-Mount, Model RFT9739). After the coriolis flow meter, the air then goes through a needle valve, which is used to regulate the amount of air flowing into the mixing section. From the needle valve, the air flows through a flexible hose, then through a one-way check valve and into the air-water mixing section.

3.1.3 AIR WATER MIXING SECTION

Two static mixers (Koflo, model 1-40C-4-6-2) are located at the experimental setup; one is located before the inlet thermocouple and the other one before the outlet thermocouple. The inlet static mixer has a dual function, the first to ensure that the inlet measured temperature accurately represents the temperature for the two-phase mixture, and the other function is to guarantee that the flow patterns observed in the visualization section are not influenced by the inlet geometry or any induced flow pattern. Refer to Figure 6 for details.

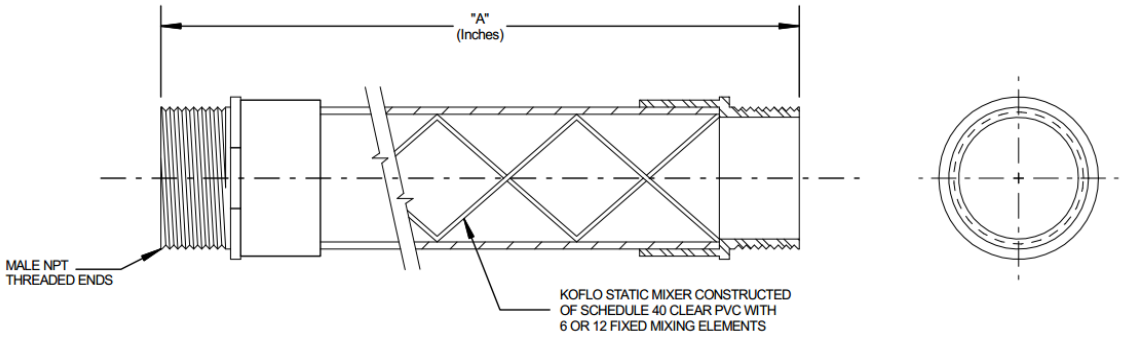

Figure 6 Static mixer

3.1.4 DATA ACQUISITION SYSTEM

During the experiment, data is recorded and stored via a National Instruments data acquisition system. The chassis is the housing for the data acquisition system (AC powered, model SCXI 100) and it provides a low noise environment and contains components for signal conditioning, power supply, and circuitry control.

Inside the chassis, three National Instruments modules are housed inside the chassis, two 32 channel SCX1102/B/C modules and one 8 channel SCX1125 module. These modules are designed for high accuracy signal conditioning of thermocouples, they can similarly be used to acquire data in millivolt, 0 to 20 mA, and 4 to 20 mA current signals. Each module contains a 2 Hz low pass filtering system in order to reduce noise from the power source. Additionally, each channel has an amplifier with a gain that can vary between 1 and 100. Input signals from 40 thermocouples, two thermocouple probes for inlet and outlet temperature, volt and current meters, and flow meters are collected and recorded.

The data recording process is performed in a CPU. LABVIEW offers a graphical interface program that was designed for the experimental setup. Data such as inlet, outlet, surrounding, and test section surface temperatures, pressure drop, system pressure, air and water mass flow rates,

superficial gas and liquid Reynolds numbers are shown in this visual interface (VI). The visual interface provides features to record data, as well as instrument to monitor the process through charts, level meters, dials and numerical indicators.

The original program was written for a different two phase flow setup by Jae-Yong Kim, a former Ph.D. candidate. Modifications were made on the basic structure of this program, so as to acquire the correct signals for thermocouples, as well as liquid and gas (low, medium and high) flow meters.

3.1.5 UPWARD AND DOWNWARD FLOW SYSTEM

In order to obtain upward or downward flows, the direction of the flow is required to be changed accordingly. A pipe installed below the setup serves as a return line for the downward flow and a supply line in the case of upward flow. See both diagrams in Figures 7 and 8 for downward and upward flow, respectively.

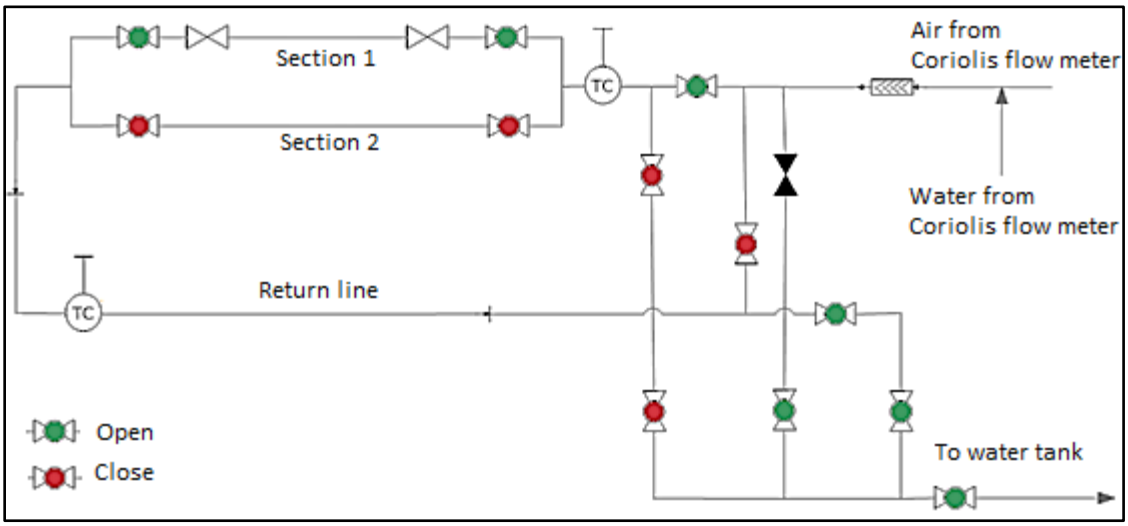

Figure 7 Downward flow diagram (valves configuration)

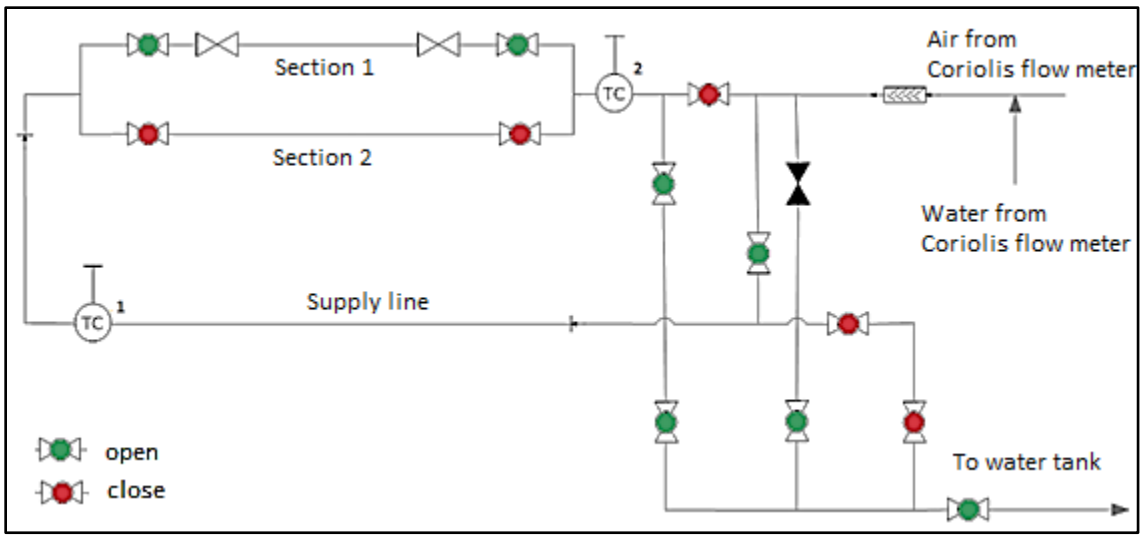

Figure 8 Upward flow diagram (valves configuration)

Additionally, several valves were installed so as to control the flow direction. Figures 7 and 8 show the specific position of the valves for each of the flow direction configurations (downward or upward). Note that green refers as open and red as closed.

3.1.6 SMOOTH PIPE SECTION

This section consists of a 25.4 mm diameter smooth transparent pipe. A detailed schematic is shown in Figures 7 and 8. Notice that section 1 refers to the smooth pipe section. The smooth pipe is used for flow visualization, pressure drop and void fraction. In order to assure a fully established flow and prevent any induced flow pattern, a calming section is used after the static mixer. This calming section is 100 inches (length to diameter ratio L/D of 100).

FLOW VISUALIZATION SECTION

The observation section starts after the calming section and consists of a 25.4 mm diameter transparent pipe with length of 304.8 mm (3ft). A high speed camera is used for the observation of the flow patterns, by acquiring videos and photographs through a computer. The lighting used

for capturing the images on the camera was established behind the clear pipe as shown in the Figure 9.

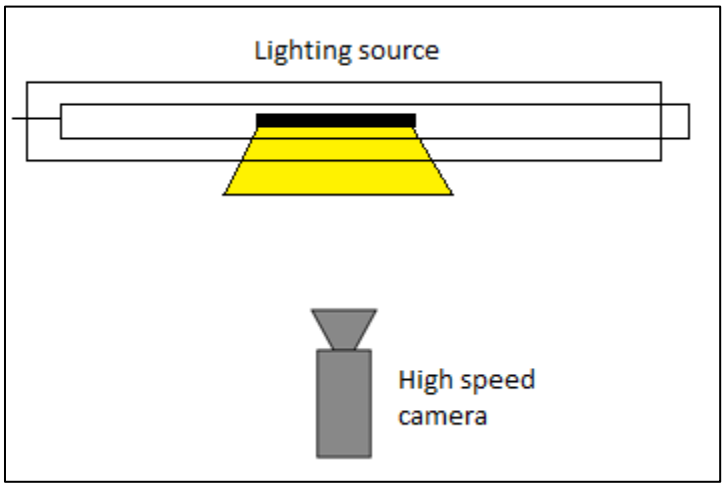

Figure 9 Flow visualization and lighting source.

VOID FRACTION SECTION

This section consists of three pneumatic quick closing solenoid valves (Dwyer Instruments, Inc. ABV1DA104SVVC) two of them were set in normally opened position while the other one was set in the normally closed position. The valves are actuated pneumatically through a solenoid valve, which is electrically excited through an electric power line of 120 VAC. The cycle time per 90 degrees of these valves is 0.03 seconds. Air pressure is required for the operation of the quick closing mechanism, according to the manufacturer this pressure is in the range of 80psi – 130 psi.

PRESSURE DROP MEASUREMENT SECTION

Pressure drop is measured between two pressure taps separated 304.8 mm (3ft) from each other. This section begins after the calming section at 100 L/D (length to diameter ratio) for downward and upward flow configurations. The pressure drop is measured using Validyne DP15 differential pressure transducer, which is connected to a Validyne CD15 carrier demodulator. The output

signals from the differential pressure transducer are demodulated and filtered through the Validyne CD15 carrier demodulator and sent to the data acquisition system for data processing.

3.1.7 ROUGH PIPE SECTION

This section is parallel to the smooth test section and it is referred as section 2 in Figures 7 and 8. It consists of a stainless steel pipe, where pressure drop and heat transfer studies can be performed. This section formed part of the old experimental setup designed by Tang (2011). This rough pipe and associated instrumentation was kept the same and re-installed in the new experimental setup.

PRESSURE DROP MEASUREMENT SECTION

As mentioned before, the rough pipe section was part of the old experimental setup designed by Tang (2011). A number of 10 pressure taps were installed and distributed along the pipe. The separation distance between pressure taps are approximately 25.4 mm and the total number of pressure taps installed was 10. The pressure drop measurements are acquired by a Validyne DP15 differential transducer and utilizing the same data acquisition system that is used for the smooth pipe section.

HEAT TRANSFER MEASUREMENT SECTION

The experimental setup has the capability to perform heat transfer measurements, this section was developed by Tang (2011). This pipe was well equipped with the necessary instrumentation for heat transfer experimentations. For more details about the heat transfer section refer to Tang (2011).

3.2 HYDRAULIC PIVOTING MECHANISM

3.2.1 DESIGN AND STRESS ANALYSIS

The design was based on the following requirements:

- Maximum inclination angle of 20 degrees.
- Upward and downward direction of the flow.

The designed mechanism consists of a double acting hydraulic cylinder (2 inch bore diameter) and a pivoting structure (two bearing and a shaft); refer to Figure 10. The bottom part of the hydraulic cylinder is connected to the base (lower part) through a pin, with the purpose of allowing rotational movement at this point; refer to Figure 11.

The upper connection of the hydraulic cylinder to the beam was made through a special designed part; refer to Figure 12. This special part is fixed to the beam through 10 bolts and to the hydraulic cylinder through one pin, which allows rotational movement at this point. Also, the part was designed considering the 25.4 mm diameter return line, which passes below the beam.

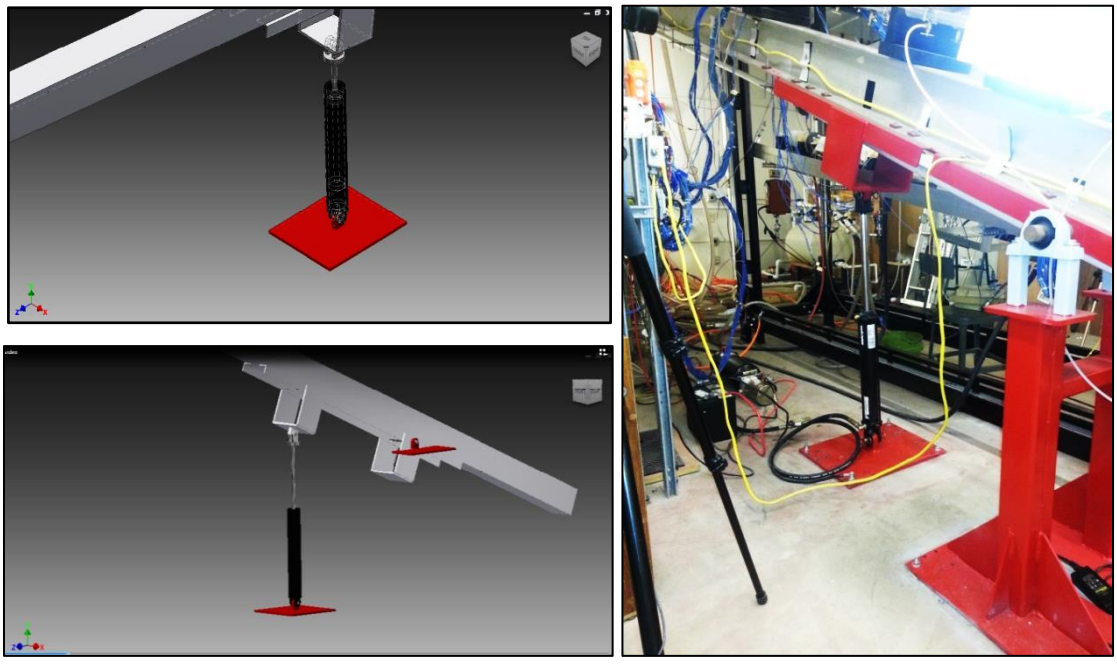

Figure 10 Left: Designed mechanism (3D model) and Right:Designed mechanism

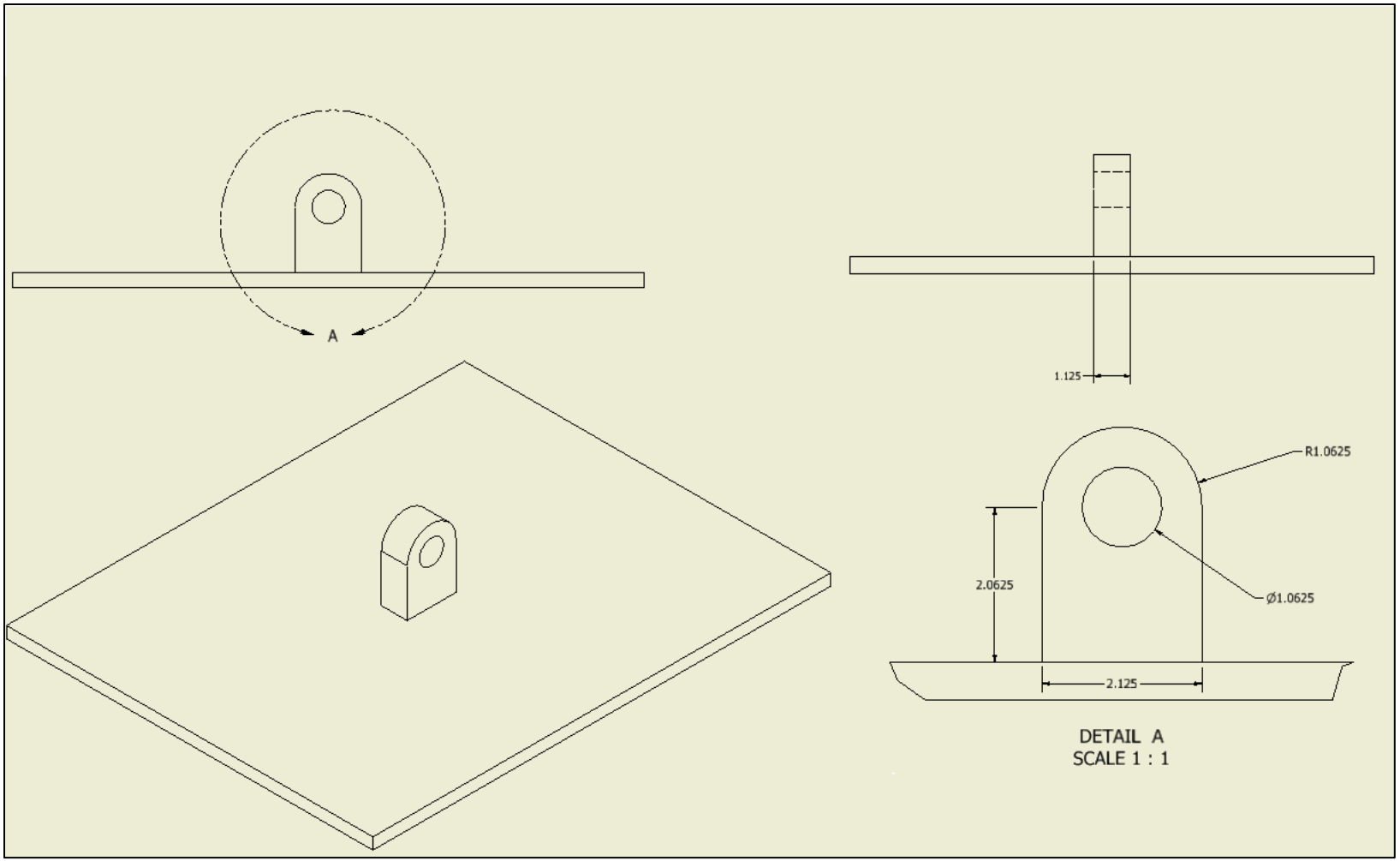

Figure 11 Lower part (connection hydraulic cylinder to the ground)

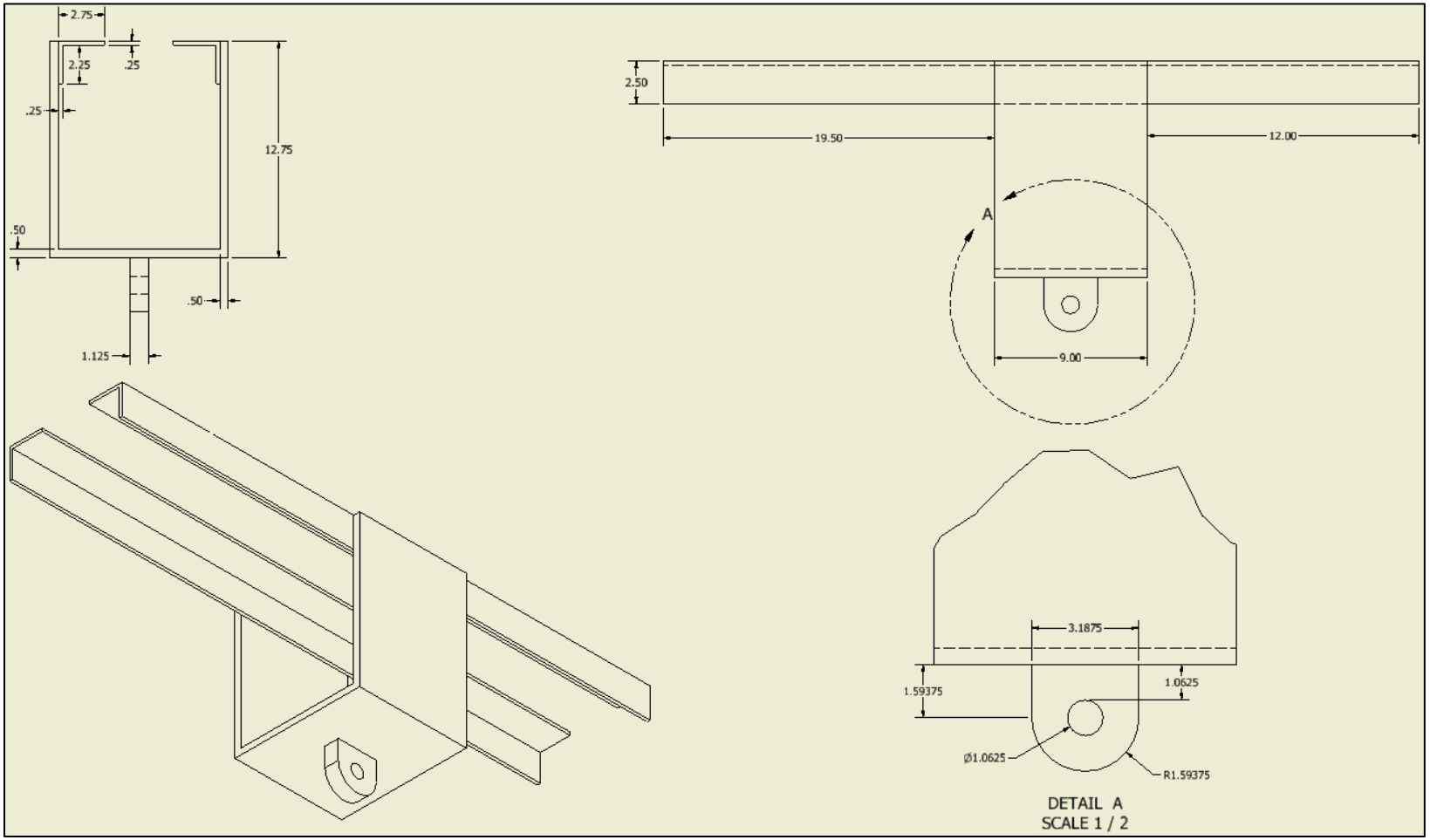

Figure 12 Upper part (connection hydraulic cylinder to the beam

The simulation of the mechanism was obtained through a 3D modeling of the system in Inventor Autodesk. The purpose of the simulation was to understand how these rotational and linear motions would affect the overall design, obtaining the displacements magnitudes in x, y and z directions; lastly this model served for the purpose of performing the stress analysis.

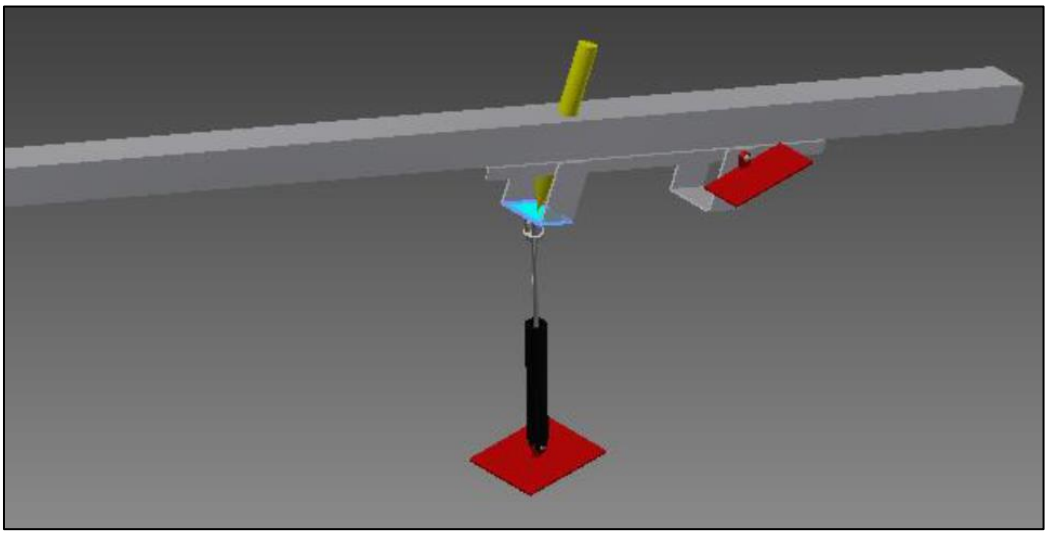

Figure 13 Stress analysis (Load)

The stress analysis was performed by applying a force of 150 N on a point shown as in Figure 13, this force applied in the simulation is much higher than the weight associated with the instrumentation acting at this point. The purpose was to verify the design in a critical condition, and the results showed that the safety factor for the system was approximately equal to 15, in almost all the structure and mechanism. Also, it was found a minimal critical safety factor of 6 at the pivoting point, which is still very safe. Please refer to Figure 14.

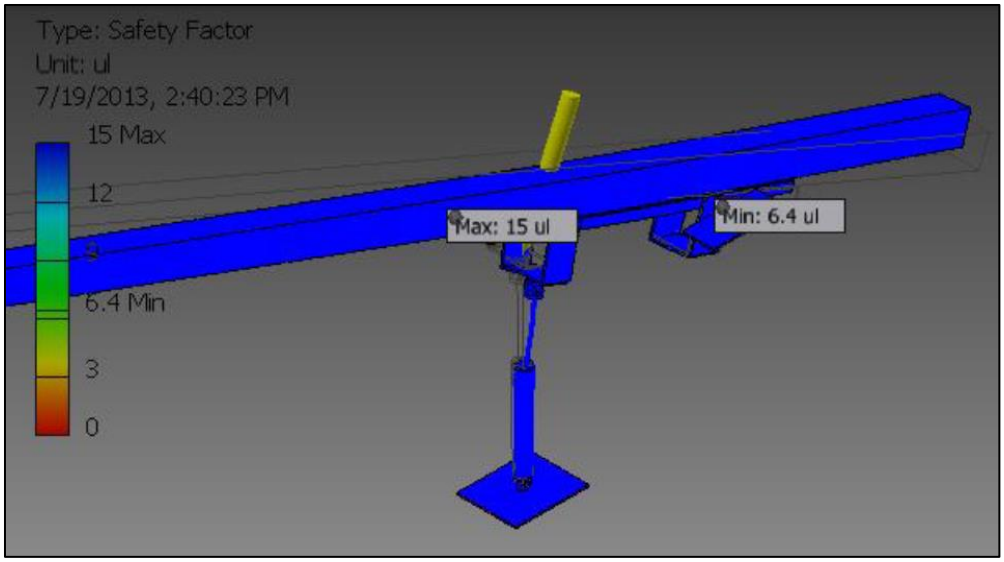

Figure 14 Safety factor of the mechanism

3.2.2 HYDRAULIC CYLINDER

The hydraulic cylinder was selected in accordance to the following:

- Loads associated with the beam and parts of the designed mechanism.
- Stroke of the hydraulic cylinder, in order to achieve the maximum inclination angle of 20 degrees.
- Type of hydraulic cylinder, geometry and freedom of motion considerations.

A 2 inch Maxim double acting tie-rod cylinder was carefully chosen. It has a stroke of 16 inches and a retracted length of 26.25 inches. When fully extended the hydraulic cylinder reaches a length of 42.25 inches. Figure 15 illustrates the chosen hydraulic cylinder.

Also, Figure 16 shows an AutoCAD drawing with all the dimensions considered for the selection. At the left side and above the beam is the air duct, and at the right side and below the beam is the floor. These dimensions were all carefully considered so as to dimension the hydraulic part.

Furthermore, it is shown in the same figure that the minimum length for the hydraulic cylinder when fully extended was 41.15 inches; therefore the selected part was 42.25 inches, which exceeds the required length by 1.1 inches. Another dimension of interest was the separation between the pivoting point and the hydraulic jack, in this design the separation was 39 inches.

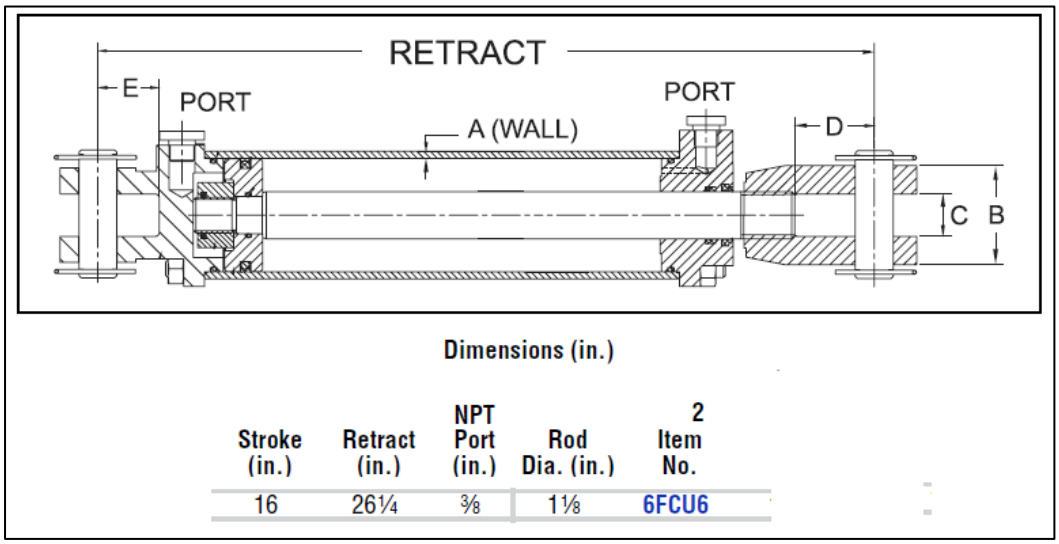

Dimensions (in.)

Stroke (in.)	Retract (in.)	NPT Port (in.)	Rod Dia. (in.)	2 Item No.
16	26¼	⅜	1⅛	6FCU6

Figure 15 Hydraulic cylinder selected for the designed mechanism

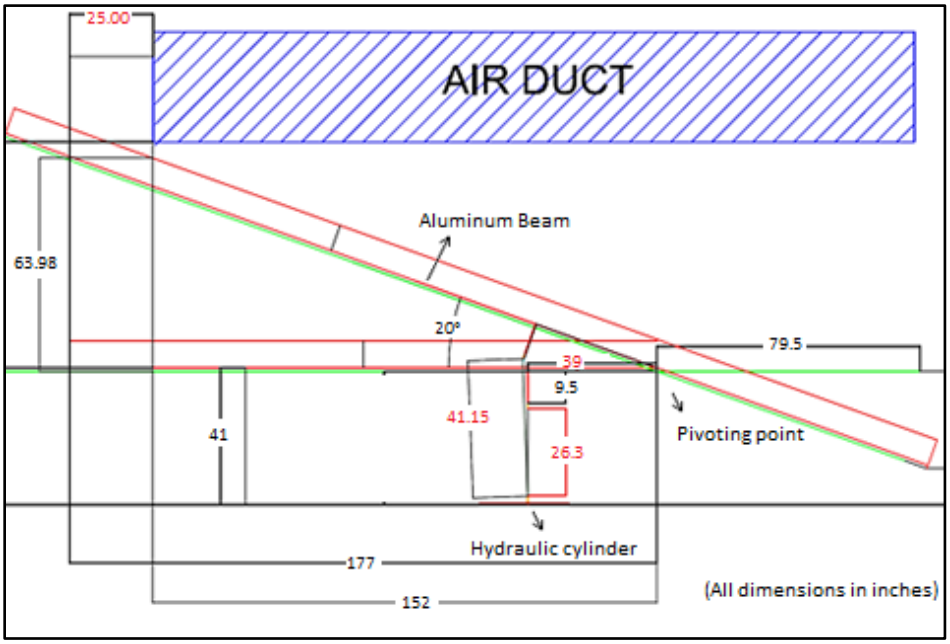

Figure 16 Dimensions considered in the design.

3.3 CALIBRATION OF EXPERIMENTAL SETUP

In this section the calibration of the different instrumentation utilized in the experimental setup are discussed. There are four instrumentation components that evoke the necessity of calibration, these are:

- Pressure transducer
- Thermocouples
- Coriolis flow meters
- Void fraction section

The calibration method for each of these four instrumentation components will be introduced in this chapter. As well as, a brief discussion of the uncertainty associated with each of the components.

3.3.1 PRESSURE TRANSDUCER

For the calibration of the Validyne pressure transducer, three different diaphragms are used in order to accurately cover the entire range of pressure drops encountered by the experimental apparatus. More precisely, the three different Validyne diaphragms corresponding to the maximum pressures are: 3.5kPa (0.5psi) or # 26, 14.0kPa (2.0psi) or # 32 and 35.0kPa (5.0psi) or #36.

In this case, calibration consists of generating a linear equation that relates the voltage output of the pressure transducer to the differential pressure that is applied. This pressure is generated at regular intervals and the voltage output from the transducer is recorded. The positive side of the pressure transducer receives the pressure, while the negative side is left open to the atmosphere. The pressure inputs are generated using a very accurate hand pump and a calibrated digital manometer, which has an accuracy of ±0.3% full scale and a resolution of 0.069 kPa (0.01 psi).

Because of its excellent resolution, this digital manometer is used for calibration of even the smaller diaphragms.

In order to obtain the calibration equation, a LABVIEW program is utilized to record the input pressures to the transducer and the coinciding output pressures. After recording these data in LABVIEW, the values can be transferred to an Excel spreadsheet where a calibration equation is generated, see Figure 17. Finally, this calibration equation is then written into the data acquisition program.

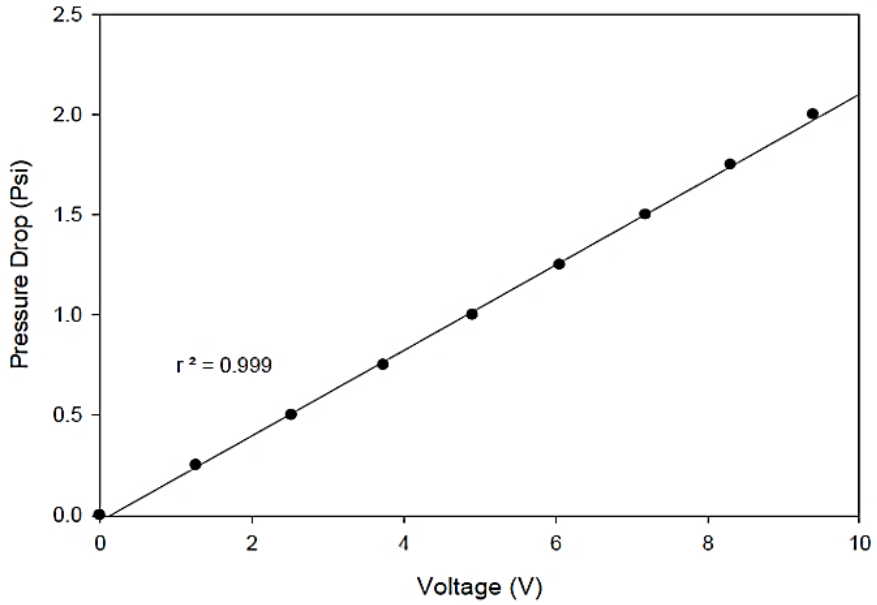

Figure 17 Calibration graph of the pressure transducer.

3.3.2 THERMOCOUPLES

The experimental setup utilizes thermocouple probes for inlet and outlet temperature measurements. These thermocouples are factory calibrated and are specified to an accuracy of ±1.0°C (1.8°F) or ±0.75% of the measured temperature value.

3.3.3 CORIOLIS FLOW METERS

The experimental setup uses two Micro Motion Coriolis flow meters; these are dispatched already calibrated from the factory. According to the flow meters specifications, when the working fluid is water, then the two CMF-025 flow meters and the CMF-100 flow meter show an accuracy of about ±0.1% of the mass flow rate.

The calibration equation is similarly obtained as in the case of the pressure transducer. The LABVIEW program is utilized to record the input pressures to the transducer and the coinciding output pressures. After recording these data in LABVIEW, the values can be transferred to an Excel spreadsheet where a calibration equation is generated. Finally, this calibration equation is then written into the data acquisition program. Figure 18 shows the calibration equation graph of the high rate air flow meter.

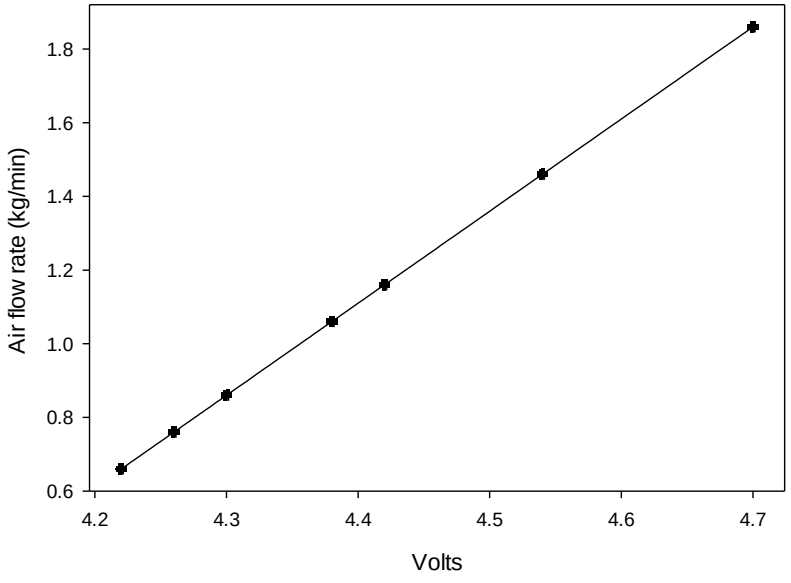

Figure 18 Calibration CMF-100 (High rate air flow meter)

3.3.4 VOID FRACTION SECTION

The calibration of the void fraction section is an essential step in order to guarantee the accuracy of the measurements obtained. Several fittings and lengths of tubing are necessary in order to route fluid to the collection tank.

Inherently, these components of the void fraction section will tend to trap some of the fluid that is drained from the void fraction section. In order to account for this phenomenon, the volume of the complete void fraction section was calculated. The volume obtained through calculation was 2290.80 cm^3 (139.80 in^3). With water as the assumed working fluid, the mass associated with this volume is 2286.21g (5.04 lbm).

Now, by performing a comparison between the volume of the total pipe section and the volume of liquid when it is completely filled with water, it was possible to estimate the amount of fluid that would be trapped in the void fraction section. The calibrated mass was calculated with the relation. $m_c = 2286.21 - m_{liq}$. It was found through this calibration process, that the amount of liquid drained from the void fraction section remained constant at a particular angle of inclination. However, it must be noted that due to the shape of the quick closing valves at either end of the void fraction section, larger amounts of fluid are trapped in the void fraction section at higher angles of inclination. Thus, it was necessary to recalibrate the void fraction section at each angle of inclination (-5, -10, -20 degrees). After proper estimates of average amount of fluid trapped in the test section at a particular inclination had been obtained, they were added to the mass of fluid drained from the test section in the form of a correction factor. Table 1 shows the amount of calibrated mass per inclination, it can also be seen that the amount of fluid trapped by the void fraction section remains relatively consistent for the different inclinations. However, the amount of fluid trapped in the void fraction section increases with increasing the inclination.

Table 1 Calculated calibrated mass for different inclinations

Pipe Orientation (θ)	**Calibrated mass (g)**
-5	170.21
-10	177.21
-20	193.21

3.4 VALIDATION OF VOID FRACTION MEASUREMENTS

In order to validate the void fraction data, a comparison was made between the present study and predicted data from various correlations. From the fourth chapter the best performing correlations based on lowest RMS were selected for this comparison. The total data points acquired in the present study was 120 points, in three different inclinations -5^{o}, -10^{o} and -20^{o}. A total of 70 points were selected from the total of 120 points in all inclinations. The void fraction correlations studied for the purpose of validation were: Gomez et al. (2000), Guzhov et al. (1967), Bhagwat and Ghajar (2013), Smith (1969), Woldesemayat and Ghajar (2007) which had the respectively RMS errors: 9.1, 11.2, 11.8, 11.9, and 12.8. In the case of Yashar et al. (2001) it was added because of its good performance at low ranges of void fraction. These correlations predicted the data within ±15% accuracy for the range of void fraction between 0 and 0.5, refer to Figure 19. While, at the range of 0.5 to 1 (Figure 20) the prediction error percentage was even at a lower value of 7.5%.

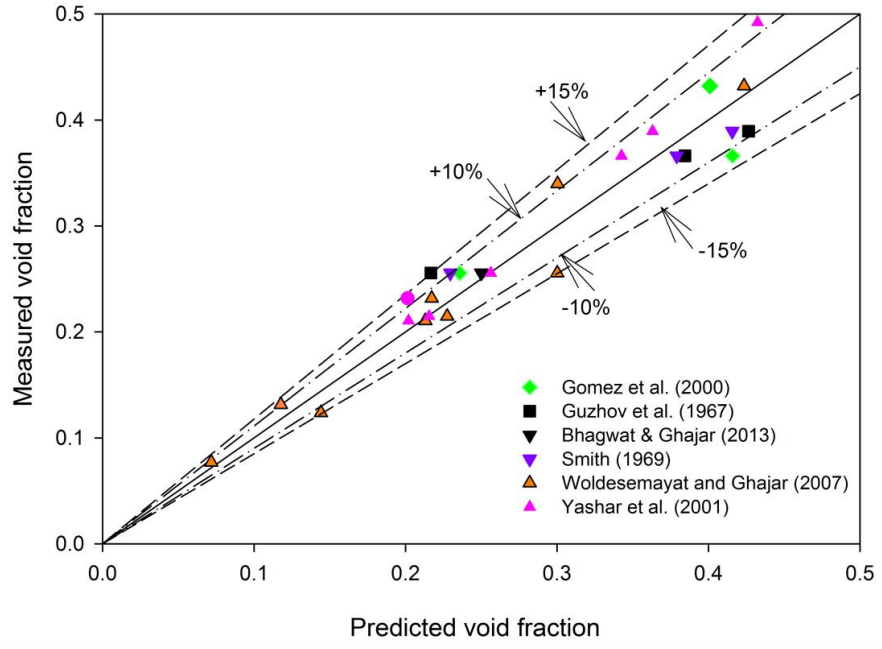

Figure 19 Comparison of measured void fraction with six best performing correlations (0 <α<0.5)

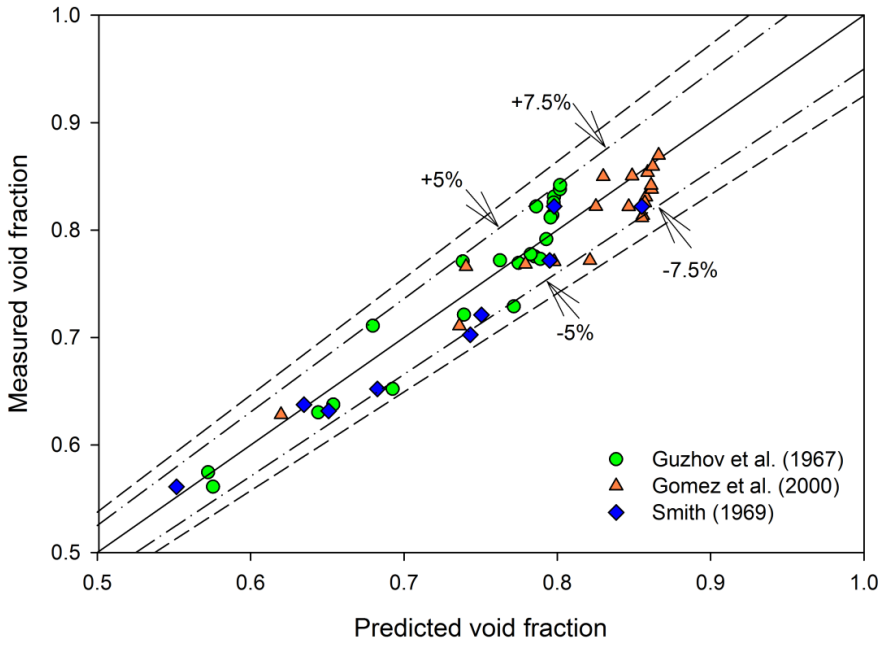

Figure 20 Comparison of measured void fraction with six best performing correlations (0.5 <α<1)

Additional validation of the measured void fraction was done by direct comparison with void fraction data from other authors. In order to proceed with the direct comparison, the pipe diameter dependency must be eliminated. Therefore, the parameter of comparison used was the mass flow rates, which eliminates the pipe diameter influence. This considers the cross sectional areas and depends only on superficial velocities and densities. Direct comparison of measured void fraction data with other sources are within ±3% error bands, as shown in Figure 21.

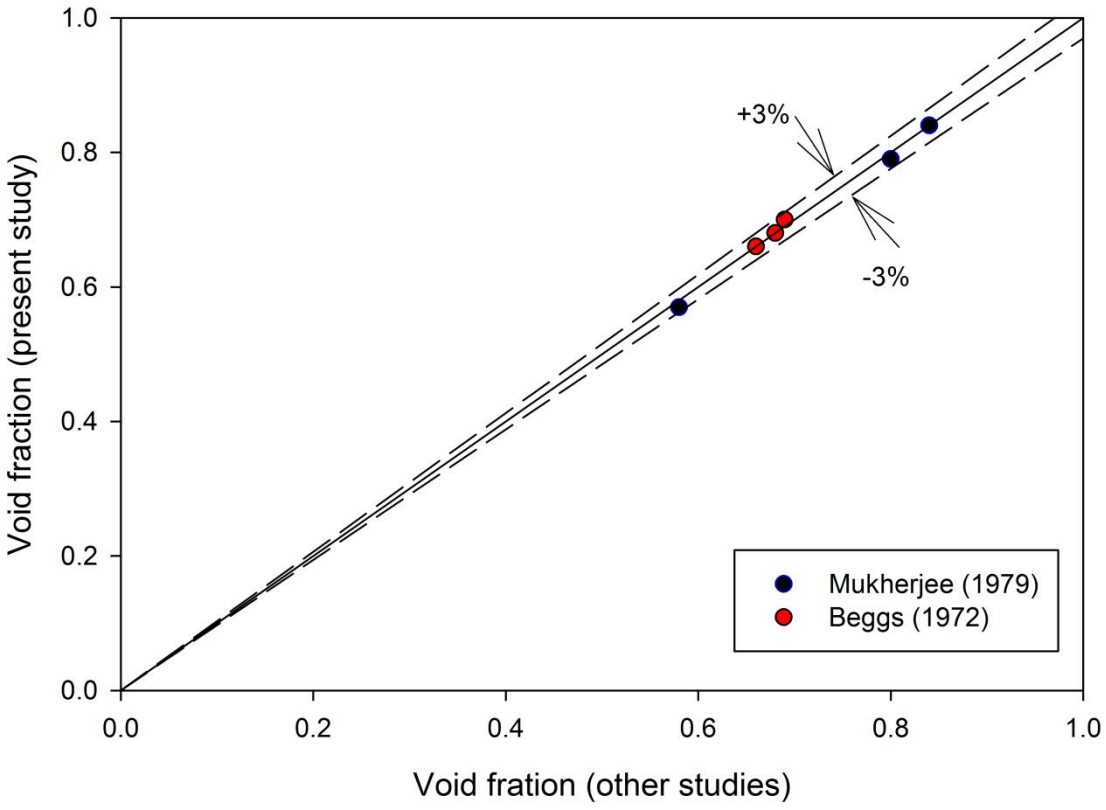

Figure 21 Comparison of measured void fraction with other studies (upward pipe orientation)

3.5 UNCERTAINTY ANALYSIS

3.5.1 VOID FRACTION DATA

The void fraction expression in terms of volume can also be expressed as a function of masses. The following expression was generated for the void fraction of the experimental apparatus:

$$\alpha = 1 - \frac{m_{liq}}{m_{tot}} \quad (1)$$

In this equation, m_{liq} represents the mass of the liquid drained from the test section into the collection tank. The term m_{tot} represents the total mass of liquid that can be contained within the test section. The value m_{tot} has an estimated uncertainty of ±2.0g.

In the case of the uncertainty of the liquid the formula for m_{liq} is as given as follows:

$$m_{liq} = m_{tank+liq} - m_{tk} + m_{cal} \quad (2)$$

where m_{cal} is referring to the liquid that has not been able to drain out from the test section and always stays inside the system. In order to acquire this calibration value the test section is filled completely with liquid utilizing high liquid flow rates. After the pipe is fully filled of flowing water, the fluid is trapped and m_{cal} is then the difference between the m_{tot} and this trapped mass of liquid.

The uncertainty related with the calibration mass is associated to the inclination angle of the experimental setup. For the purpose of this investigation, the maximum observed value of m_{cal} was 193.21 g at an inclination angle of -20 degrees, and which uncertainty was ±2.0 g.

It should also be noted that the mass of the fluid in the collection tank was found by subtracting the measured mass of the empty tank (m_{tank}) from the combined measured mass of the tank and the drained liquid ($m_{tank+liq}$).

Each of these masses is measured using a scale with a resolution of 1g. Hence, they each have associated uncertainties of ±0.5 g. If these measured masses and the correction factor are introduced into the void fraction equation, the following relation is generated:

$$\alpha = 1 - \frac{m_{tank+liq} - m_{tk} + m_{cal}}{m_{tot}} \tag{3}$$

The uncertainties associated with the calculation of m_{liq} are additive. Thus, for the worst case scenario, the maximum uncertainty associated with the value of m_{liq} is ±3.0 g.

The uncertainty associated with the void fraction measurement can be calculated from the following relation:

$$w_{\alpha} = \left[\left(\frac{\partial \alpha}{\partial m_{liq}} w_{m_{liq}}\right)^2 + \left(\frac{\partial \alpha}{\partial m_{tot}} w_{m_{tot}}\right)^2\right]^{1/2} \tag{4}$$

or

$$w_{\alpha} = \left[\left(\frac{1}{m_{tot}} w_{m_{liq}}\right)^2 + \left(\frac{m_{liq}}{{m_{tot}}^2} w_{m_{tot}}\right)^2\right]^{1/2} \tag{5}$$

The void fraction uncertainty is directly related to the range of the void fraction. It was found that the void fraction uncertainty changes with low or high values of void fraction. The worst case was observed at low void fraction values while the best case was related to higher void fraction values. Added to this, uncertainties were observed to be sensitive to pipe inclination angle as well.

Table 2 Void fraction uncertainty for -5, -10 and -20 degrees

Inclination angle	Uncertainty	Liquid flow rate (kg/min)	Gas flow rate (kg/min)	Void fraction range
-5	±3.90%	70	0.0015	0.04
	±0.17%	10	0.80	0.84
-10	±2.00%	70	0.0015	0.08
	±0.15%	10	0.90	0.90
-20	±2.00%	70	0.0015	0.08
	±0.15%	5	0.90	0.88

As shown in Table 2, the minimum uncertainty of ±0.17% was calculated at the highest void fraction in each of the inclinations. However, lower values of void fraction gave greater percentages of uncertainty. The highest uncertainty was ±3.90% for the case in which the pipe is at -5 degrees of inclination.

3.6 EXPERIMENTAL PROCEDURES

The experimental procedure presented in this chapter served to ensure the safety of the user as well as the integrity of the setup during the data taking process. Additionally, allows reducing the errors and increases accuracy of the data obtained. Operation of the experimental setup can be divided into four different major sections, independent of the type of data being collected: System Warm Up, Data Collection (for each research mode), and System Shut Down.

Also, the following procedures regarding the operation of the experimental setup are presented in seven sections:

- Flow direction settings
- System warm up
- Flow visualization

- Pressure drop measurements
- Heat transfer measurements
- Void fraction measurements
- System shut down

Although the general operation of the experimental setup for each of these modes is quite consistent, in many aspects they are unique. Therefore, exclusive procedures are required. The chapter will present all of the procedural aspects associated with the operation of the experimental apparatus, as well as a discussion on the data collection for each of the research modes.

3.6.1 FLOW DIRECTION SETTINGS (UPWARD OR DOWNWARD FLOW)

The flow direction will depend on the interest of study, whether the concentration is on downward or upward flows. The flow direction can be established on the setup by opening and closing an array of ball valves that will ultimately set the direction of the flow. The steps for the flow direction setup are presented as follows:

1. Open the return valve that will allow the flow to go back to the tank. There is one return valve for downward flow and another one for upward flow. Make sure to open the correct one. The valves are labeled indicating which one is the upward or downward return valve.
2. Check that the return valve related to the flow direction that the user is not interested, is in the closed position.
3. Follow the flow diagram in order to open and/or close the corresponding ball valves for each flow direction setup. Follow the valves configurations on Figures 22 and 23, in which green means that the valve needs to be open and red, that it needs to be closed.

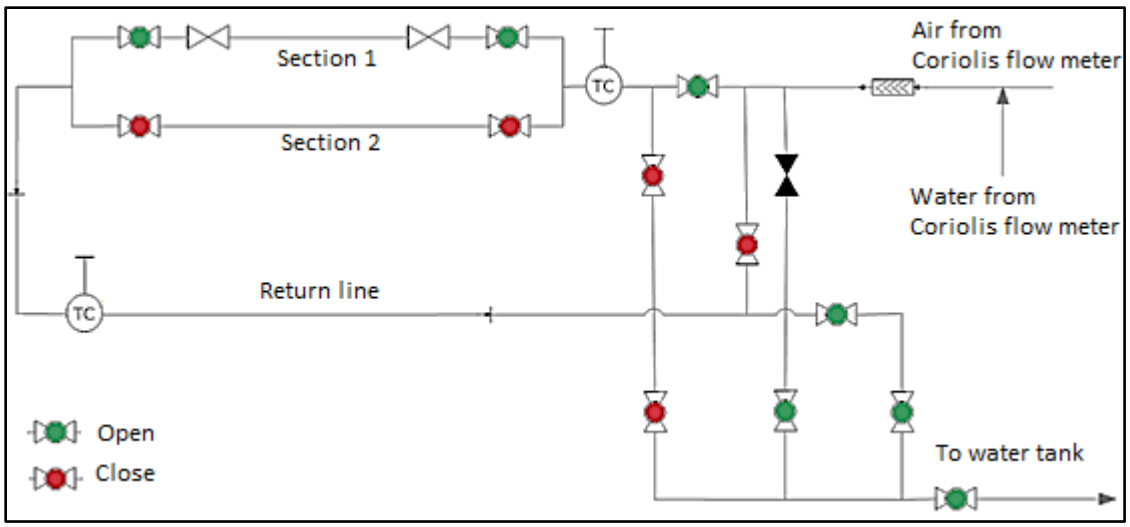

Figure 22 Downward flow diagram (valves configuration)

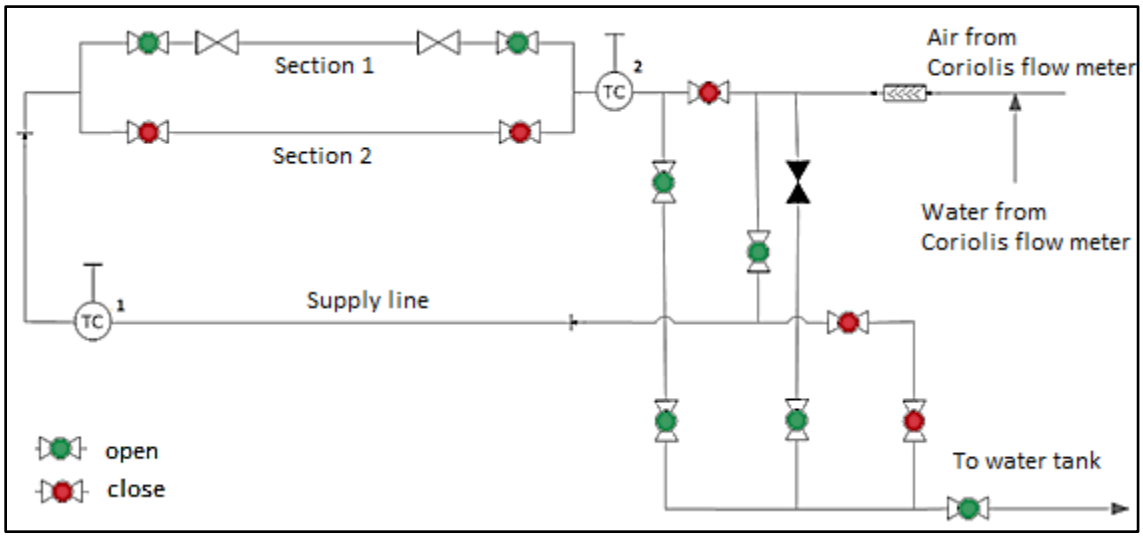

Figure 23 Upward flow diagram (valves configuration)

3.6.2 SYSTEM WARM UP

The system warm up consists of the previous steps that should be taken prior to initiation of any measurement activity.

1. Turn on the flow meters.
2. Turn on Demodulator and power supply for pressure transducer.

3. Initiate the LABVIEW program. Select the proper program depending on the gas flow rate meter used. There are three programs: low, medium and high flow rate.
4. Turn on air compressor.
5. Open main line shutoff valve for the compressor.
6. Check the pressure at the pressure regulator. The pressure should indicate more than 90 psi.
7. Open the valve one quarter turn for the water heat exchanger. This drops the temperature of the liquid into the system.
8. Check the bypass vale of the pump. It should always be partially open. This allows water to circulate properly.
9. Open the valve which supplies liquid to the apparatus. There is one for the half inch and one for the one inch experimental setup.
10. Connect the differential and absolute pressure transducers.
11. Open quarter turn the cutoff valves for both the air and water lines.
12. Adjust the liquid mass flow rate through the manual control valve.
13. Bleed the inlet and outlet of the pressure transducers in order to remove any air bubbles (Only liquid should run in the system).
14. Adjust the air flow rate through the manual control valve.
15. Check for any leakage.

3.6.3 FLOW VISUALIZATION

The procedure for performing flow visualization is as follows:

1. The light equipment should be placed at the back of the transparent pipe.
2. Adjust the light intensity of the lighting equipment.
3. Connect the power to the lighting equipment.

4. Set the camera or video camera in front of the transparent pipe.
5. If utilizing video camera, then open the video camera software Motion Studio for recording the video and observe the flow.
6. Take photographs adjusting lighting in the room and changing the flash setup in the camera.

3.6.4 PRESSURE DROP MEASUREMENTS

The procedure for performing pressure drop measurements is as follows:

1. Once the flow rates are set, wait 2 to 3 minutes for the system to stabilize.
2. Then run the LABVIEW program and save the run with the proper identification number.
3. Press the record data bottom in LABVIEW and record data for 2 to 3 continuous minutes.
4. After recording data time has passed, press the stop bottom in the LABVIEW program.

3.6.5 HEAT TRANSFER MEASUREMENTS

Refer to Tang (2011) for a detailed method on heat transfer data measuring process.

3.6.6 VOID FRACTION MEASUREMENTS

The following is the general procedure for the collection of void fraction data:

1. Once the flow rates are set, wait 2 to 3 minutes for the system to stabilize.
2. Then run the LABVIEW program and save the run with the proper identification number.

3. Press the record data bottom in LABVIEW and record data for 1 to 2 continuous minutes.
4. Operate the solenoid valves, by activating the electrical switch.
5. Open the outlet ball valve which serves to the collection tank.
6. Use the air pressure line connecting this to the opposite side where the water was collected. This pressurized air will push the liquid remaining in the pipe into the collection tank.
7. Measure the mass of the collected liquid with the electronic scale.
8. Take notes of the weighted mass and subtract the previous measure so as to calculate the difference which will give the liquid mass of water and therefore void fraction can be calculated from there.

3.6.7 SYSTEM SHUT DOWN

System shut down simply includes all of the steps necessary to shut down equipment and to properly clear the test section. Proper clearing of the test section is necessary in order to prevent the accumulation of organics such as algae in the system. The steps for system shut down are as follows:

1. Turn off the water pump.
2. Close the water line control valve and all quarter turn ball valves associated with the water delivery system.
3. Set the air control valve until air is flowing through the system at its maximum rate.
4. Remove all residual water from the system.
5. Shut off air flow manual control valve.
6. Close the quarter turn cutoff valve which serves to the water heat exchangers.

7. Power off the data acquisition system, demodulator and power supply of the pressure transducers.
8. Lastly, power down the air compressor.

CHAPTER IV

RESULTS AND DISCUSSION

Experimental results on downward flows are discussed in this chapter. These results cover three different near horizontal pipe inclinations (-5^o, -10^o and -20^o). Flow patterns were identified and flow maps were developed for all three pipe inclinations. Comparisons between the flow map developed in the present study and the 12.7 mm pipe diameter flow map created by Ghajar & Bhagwat (2014) were conducted. Differences were discussed by analyzing the combined effects of gravitational, buoyancy, surface tension and inertial forces acting on the two phase flow. One of the most significant differences was in the bubbly flow regime, which was not observed in the present study, oppose to the case of the 12.7 mm pipe diameter flow map were bubbly flow was perceived by Ghajar & Bhagwat (2014) at low gas and high liquid flow rates.

In order to perform evaluations on thirteen selected void fraction correlations, a total of 120 void fraction data points for downward inclinations were measured. The effect of pipe orientation on void fraction was discussed as well as the variation of void fraction with respect to flow patterns.

The performance of these correlations was evaluated and the best performing correlation based on specific void fraction ranges and pipe orientation (-5^o, -10^o and -20^o) was determined.

4.1 FLOW PATTERNS AND FLOW MAPS

Flow patterns have been investigated for decades and many flow pattern maps have been developed. However, there is not a unique procedure to identify flow patterns. The most utilized way to identify flow patterns is by performing flow visualization in a transparent pipe. Video recording and photographs are commonly used to identify the flow pattern. It is important to notice that due to the nature of the flow visualization technique, flow patterns are considered a highly subjective procedure.

Flow visualization was conducted in a 25.4 mm diameter transparent polycarbonate pipe. Both recording videos and photographs were utilized in order to evaluate each point at a certain gas and liquid flow rate. Four flow maps were obtained, horizontal and downward inclinations (-5^o, -10^o and -20^o), showing the transitions between different flow patterns. In order to compare the different transition lines on each pipe orientation, the four flow maps were concentrated in one single flow pattern map.

4.2 FLOW PATTERNS IN DOWNWARD INCLINED PIPE ORIENTATIONS

By performing flow visualization on downward orientations, four distinctive flow patterns were observed, these were: stratified, slug, intermittent and annular. The bubbly flow pattern was not observed in the present study (25.4 mm pipe diameter), in contrast to a similar study conducted by Ghajar & Bhagwat (2014) in a 12.7 mm pipe diameter. There are two possible reasons for not observing the bubbly flow in the present study: the first is that the liquid phase may not be sufficient to fill the pipe, and then the liquid phase sets at the bottom of the pipe as gravity also pulls the liquid down, causing it to accelerate and creating stratifications of the flow. The second reason may be that due to buoyancy forces the gas bubbles find space at the top of the pipe where

they colloid and form new and bigger bubbles that will ultimately become plugs or slugs, instead of spherical bubbles flowing with the flow stream. Photographs of the observed four flow patterns were taken and are shown in Figure 24. (A) $\dot{m}_l$= 27.22 kg/min, $\dot{m}_g$= 0.001 Kg/min, (B) $\dot{m}_l$= 15.88 kg/min, $\dot{m}_g$= 0.3 Kg/min, (C) $\dot{m}_l$= 29.48 kg/min, $\dot{m}_g$= 0.3 kg/min, (D) $\dot{m}_l$ = 6.8 kg/min, $\dot{m}_g$ =0.8 kg/min.

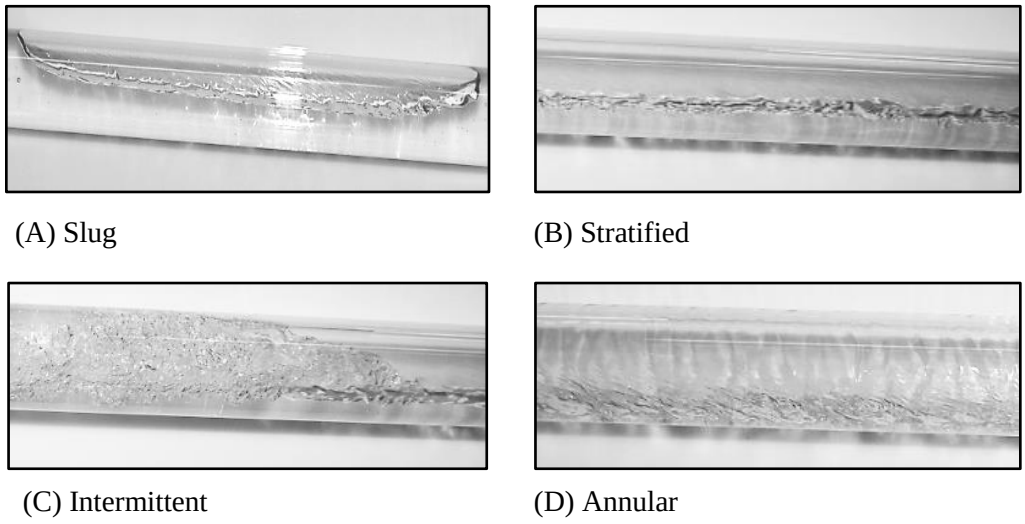

(A) Slug (B) Stratified

(C) Intermittent (D) Annular

Figure 24 Representative photographs of the four flow patterns for -5 degrees inclination.

4.2.1. SLUG FLOW

Slug flow is distinguished by cylindrical shaped bubbles that travel along with the fluid. Simmons & Harantty (2001) described the formation of slug in horizontal two phase flow as the passes by which waves grow intermittently on a stratified interface, causing the liquid phase to fill the pipe cross section.

These bubbles are considerably large and have noticeable shapes. For the case of downward flow, the tip of the slug is found at the down side of the pipe. This shape is molded by the effects of buoyancy forces acting on the fluid due to gravity. It is important to mention that by changing the flow rates or the pipe inclination, the shape and size of the slugs may also change accordingly. In

Figure 25, slugs are shown at similar liquid and gas flow rates. Similar observations were also made by Oyewole (2013) in an experiment conducted in a 12.7 mm diameter pipe. Photographs (A) and (B) are at flow rates of $\dot{m}_g$= 0.003 and $\dot{m}_l$= 23.59 kg/min, (A) represents a pipe with inclination of -10^o while (B) represents stratified flow for -20^o.

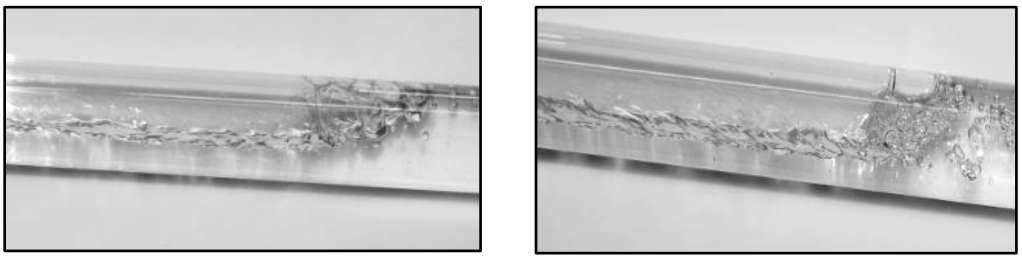

(A) -10^o (B) -20°

Figure 25 Representative photographs of different shapes slug flow pattern for -10^o and -20^o

4.2.2. STRATIFIED FLOW

Stratified flow is characterized by the separation of the liquid phase from the gas phase. The liquid is located at the bottom while the gas is traveling on the top inner part of the pipe. After performing flow visualization on downward inclinations it was observed that this type of flow was the predominant flow pattern over the other types of flow regimes which were observed in the present study.

Gravity pulls the liquid phase down the pipe causing the liquid to be accelerated. When the downward inclination angle is increased toward more negative values it is observable that the thickness of the liquid phase decreases for similar values of liquid and gas flow rates. Figure 26 shows the difference on the thickness layer of liquid in stratified flow for different pipe orientations. Photographs (A) and (B) are at flow rates of $\dot{m}_g$= 0.005 and $\dot{m}_l$= 16.24 kg/min, (A) represents a pipe with inclination of -5^o while (B) represents stratified flow for -20^o. In Figure 26, it is clearly observable how despite gas and liquid flow rates been the same, when changing the

inclination angle the thickness of the liquid phase on the two phase flow changes also. For the case of -20^{o} the thickness is less, as previously mentioned gravity acts on the liquid phase causing it to accelerate and more liquid is able to escape off the pipe, decreasing the observable thickness of the liquid phase on the stratified flow.

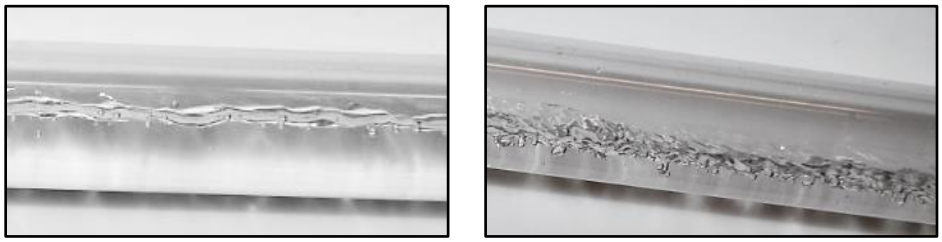

(A) -5° (B) -20°

Figure 26 Representation of stratified flow for -5^{o} and -20^{o} at $\dot{m}_g$= 0.005 and $\dot{m}_l$= 16.24 kg/min

4.2.3. INTERMITTENT FLOW

Intermittent flow regime is characterized by periodic waves that flow through the pipe. These waves are very turbulent and the gas and liquid phases are well mixed. There are two types of intermittent flow patterns; the first is when the liquid flow rate is considerably high (>20 kg/min) and the second is for low to moderate liquid flow rates (1 kg/min - 20 kg/min).

The first type can be considered as wavy type of slugs that flows very fast carrying turbulence with them and causing the pipe to be wet in its perimeter. Often these waves are confused with annular flow since once the turbulent wave flows through the pipe; it forms a thin layer of liquid at the wall around the perimeter of the pipe, creating what may look like an annular flow pattern. In Figure 24 photograph (C) is a representation of this type of flow.

The second type is related to the stratified flow. When stratified flow is obtained and gas flow rates are increased until a moderate value (0.5 kg/min – 0.8 kg/min), then the flow reaches the transition to intermittent (refer to the flow map section). This type of flow is also called wavy

flow, and waves often touch top part of the pipe. Also larger and turbulent types of waves were observed for this type of regime comparable to the ones observed in type one.

These two types of intermittent flows are very similar. However, the gas flow rates range in which this regime is observed changes per orientation, details about the transition lines to intermittent flow regimes, are well discussed in the flow map section.

4.2.4. ANNULAR FLOW

Annular flow is characterized by a continuous thin film of liquid in contact with the pipe wall and the gas phase at the core of the pipe. This flow regime was observed at high gas flow rates approximately (> 0.9 kg/min), regardless of the liquid flow rate. Even with a low liquid flow rate, if the gas flow rate is significantly large then an annular flow will be produced. The gas pushes the liquid outwards towards the pipe wall.

It was observed that although the fluid is forming a thin film layer at the pipe wall, at the bottom of the pipe the liquid thickness was greater than at the top. This is caused by gravity forces acting on the liquid phase and forcing it to concentrate even more at the bottom of the pipe wall. Figure 27 shows a representation of annular flow regime observed at $\dot{m}_g$= 0.8 kg/min and $\dot{m}_l$= 9 kg/min and -5^o

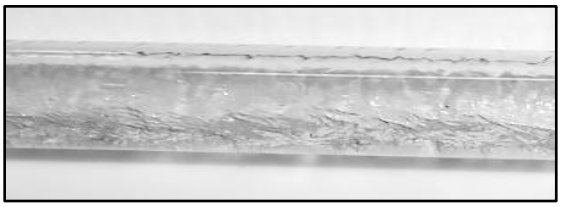

Figure 27 Representation of annular flow pattern at -5^o

4.3 FLOW MAP

Flow pattern maps are graphical representations of the different flow patterns. Flow maps are used to identify the flow pattern that may be produced under certain conditions. Different parameters have been used in order to plot these flow patterns, like the ones shown in the flow map section of the literature review in Chapter II. In order to avoid any dependency of flow parameters on any fluid property, mass flow rates of liquid and gas were used as the identification parameters on the flow maps.

Identification of flow patterns is a subjective topic as mentioned before. Often it depends on the investigators ability to identify the flow regime. In order to improve the accuracy of categorizing each flow pattern, a high speed camera was used. Since the camera recorded videos in which the fluid could be analyzed in slow motion, then the camera allowed recognizing the flow patterns which were formed by high mass flow rates, making the flow pattern identification process more reliable and accurate.

Ghajar & Bhagwat (2014) developed a flow map for downward inclinations on an experimental setup of 12.7 mm pipe diameter. Superimposing four different flow maps for different orientations, transitions lines from one flow pattern to another were compared in the same flow map. Figure 28 shows the flow map developed by Ghajar & Bhagwat (2014) for 0^o, -5^o, 10^o, -20^o.

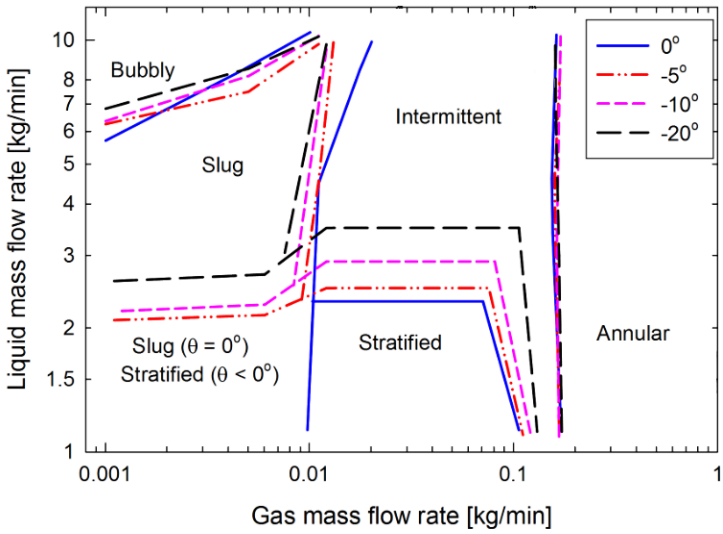

Figure 28 Downward flow map developed by Ghajar & Bhagwat (2014)

In the present study flow visualization was performed with the aid of a video recording high speed camera, a flow map was developed showing four different pipe orientations, 0^o, -5^o, -10^o and -20^o as shown in Figure 29.

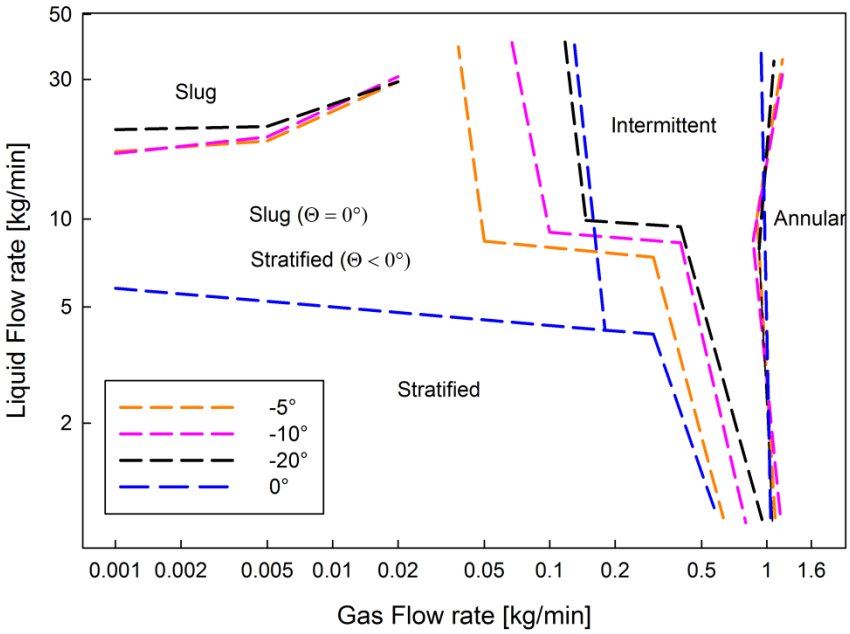

Figure 29 Downward flow map showing 0^o, -5^o, -10^o& -20^o flow pattern transition boundaries.

Barnea (1987) reported that the liquid phase in downward flows is accelerated by the gravitational force acting in the direction of the flow. She also mentioned that for downward inclinations the fluid in stratified flow moves more rapidly than in horizontal orientations. Due to this same effect, the liquid film thickness is less for downward orientations. Since the fluid is moving faster, then more amount of fluid exits the pipe and the film thickness is consequently reduced. For this reason the transition line from stratified region to slug flow is shifted up for the case of downward flow (black, orange and pink lines) compared to horizontal (blue line) as shown in Figure 29.

It is also shown in Figure 29 that the transition lines from stratified to slug for downward orientations (black, orange and pink lines), are almost identical. However, there is a small shift up of these transition lines when the inclination angle is increased towards the negative values. Again, this is due to the acceleration of the liquid phase due to gravity.

The transition lines from stratified to intermittent flow in the case of downward orientations are well illustrated in Figure 29. Lines shifted from left to right in the case when increasing the gas flow rates, and these are ordered from left to right as follows: -5^{o} (orange), -10^{o} (pink) and -20^{o} (black). As described by Barnea (1987) when the pipe is in the downward position, the liquid phase is accelerated and as consequence a thinner film of liquid is observed at the bottom of the pipe. For this reason when the inclination angle increases towards negative values, the effect of gravity on the fluid is more, thus the fluid when accelerated generates less liquid available at the bottom of the pipe. Hence, higher inclination angles require greater values of gas flow rates in order to re-arrange the liquid which is available in the pipe to produce an intermittent flow regime.

It is important to notice that for the horizontal transition line from stratified to intermittent flow (blue line), two cases were observed. The first case is when the two phase fluid is stratified flow

and while maintain constant liquid flow rates and increasing the gas flow rates it becomes an intermittent flow. The second type is for higher liquid flow rates ($\dot{m}_l$= 7.5 kg/min), similarly the transition occurs but in this case from slug regime to intermittent flow.

In the case of annular transition lines, they are almost at the same gas flow rate regardless of the orientation. It is noticeable from Figure 29 that this transition line occurs approximately at $\dot{m}_g$= 0.9 kg/min

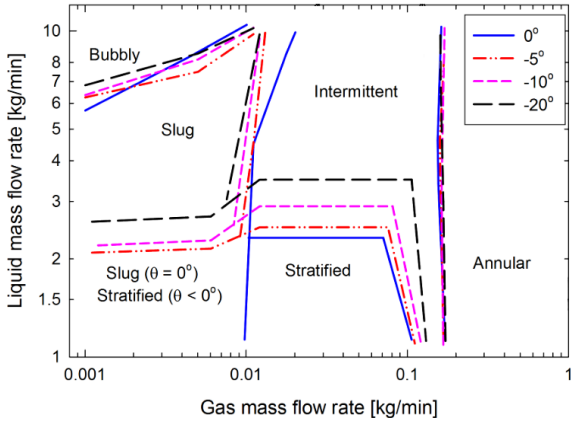

(A)

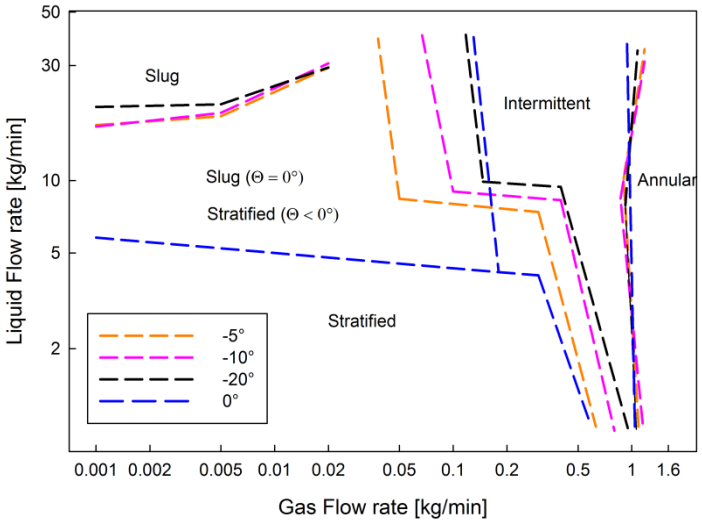

(B)

Figure 30 Comparison of flow maps between (A) Ghajar & Bhagwat (2014) (12.7 mm diameter pipe) and (B) the present study (25.4 mm diameter pipe) for downward two phase flow.

The flow map developed in the present study for a 25.4 mm pipe diameter, differs from the one established by Ghajar & Bhagwat (2014) for a 12.7 mm pipe diameter as shown in Figure 30. By performing this comparison, the influence that the pipe diameter has on the formation of flow patterns was established. The first difference that can be observed in Figure 30 is that the mass flow rate spans of both flow pattern maps are different. The 25.4 mm flow map has expanded in the gas and liquid flow rate axes.

The most noticeable difference between the 12.7 mm and 25.4 mm flow pattern maps is on the stratified flow region. It is observed in Figure 30 how the area that represents the stratified flow regime on the 25.4 mm flow pattern map is greater than the one shown for the 12.7 mm pipe. This is due to the pipe diameter difference, thus a larger volume of the pipe that is needed to fill up by the liquid, therefore the stratified flow pattern area for the 25.4 mm pipe is significantly larger in comparison to the 12.7 mm.

Another noticeable difference shown in Figure 30 is on the transition line between stratified and slug flow. For the 25.4 mm pipe this transition line is shifted up in comparison to the 12.7 mm pipe flow pattern map developed by Ghajar & Bhagwat (2014). The reason for the movement of this transition line is strictly related to the pipe diameter. With large pipe diameter, more liquid is needed to fill up the pipe and slugs are not produced until the liquid has reached certain level. For the case of 12.7 mm pipe diameter the slugs were formed at around $\dot{m}_l$ = 2.5 kg/min according to the flow map developed by Ghajar & Bhagwat (2014). On the other hand, it was observed on the 25.4 mm pipe that the necessary liquid to develop slug flow was approximately at a value of $\dot{m}_l$= 18.5 kg/min.

4.4 VOID FRACTION

Void fraction measurements were conducted on downward flows. These data was analyzed and discussed in this section. One of the analyses performed with the acquired data was the evaluation

of the effect of flow patterns in void fraction measurements. This effect showed the dependency of void fraction values on flow patterns.

Additionally, void fraction data was acquired on different orientations so as to study the influence of downwards inclinations on void fraction measurements. Graphs were obtained in order to exemplify this effect at three different inclinations ($-5^{o,}$ -10^{o} and -20^{o}).

Also, an extensive evaluation was accomplished on thirteen well-known void fraction correlations, available in the literature. The assessment was made at different inclinations, and the best correlations are highlighted depending on the range of applicability on which they performed the best.

This investigation also attempts to investigate the pipe diameter influence on void fraction. Therefore, a comparison was done between the present study and a similar investigation performed by Oyewole (2013) which studied void fraction in 12.7 mm pipe. This comparison served to determine comparison on the performance of void fraction correlations. Therefore, the pipe diameter sensibility was evaluated by performing this contrast.

4.4.1 VARIATION OF VOID FRACTION WITH FLOW PATTERN

Void fraction dependency on flow patterns was observed in the experiments at different downward inclinations. For instance, in the case of slug flow, the amount of gas in the mixed flow was small compared to stratified or annular flow. Therefore, the void fraction in slug flow is less than the other flow patterns. This flow pattern dependency on void fraction was established by performing void fraction measurements and utilizing the flow pattern map which was developed for downward inclinations. Refer to the previous section for further details about the flow pattern map.

The variation of void fraction with flow pattern is shown in Figures 31, 32 and 33 for 5^o, -10^o and -20^o inclinations respectively. These values were able to be obtained by maintaining constant liquid flow rates while increasing the gas flow rate. For the slug region the upper limits of void fraction remains constant at the value 0.40, this is show in Tables 3, 4 and 5 for -5^o, -10^o and -20^o inclinations respectively. For the case of stratified, the upper limit changes from 0.84 to 0.87 when increasing the downward inclinations. The experimental uncertainties associated with the stratified upper limits are: ±3.90 %, ±2.00 % and ±2.00%, for 5^o, -10^o and -20^o inclinations respectively. For more details refer to uncertainty analysis in Chapter III. Hence, the void fraction values are within experimental uncertainty. The increment of the void fraction upper limit in the case of -20^o was due to the increased velocity of the fluid, which is influenced by the gravity. This is also explained in the explanation for the shifting of transition lines in the flow pattern map section.

The upper limit in the case of annular flow increases from 0.87 to 0.92, for the cases of inclinations -5^o and -10^o, respectively. These values fall within the values of uncertainty for high void fraction. The transition lines to annular flow regime observed in the flow pattern map showed almost a vertical line across the liquid gas flow rates and also they are very close to each other. This explains how regardless of inclination at annular flows the void fraction is independent of the inclination.

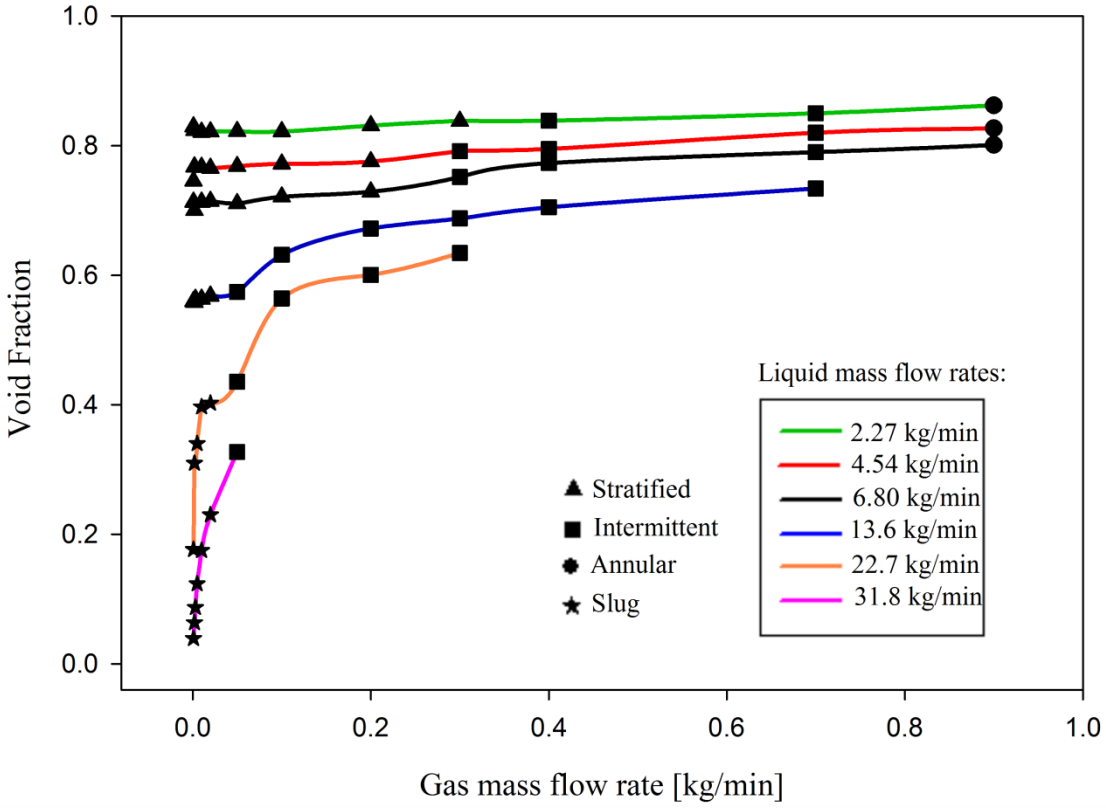

Figure 31 Variation of void fraction with flow pattern -5°

Table 3 Range of void fraction for distinct flow patterns observed in present study for -5°

Flow pattern	**Range of void fraction**
Slug	0.04 - 0.40
Stratified	0.55 - 0.84
Intermittent	0.38 - 0.85
Annular	0.80 - 0.87

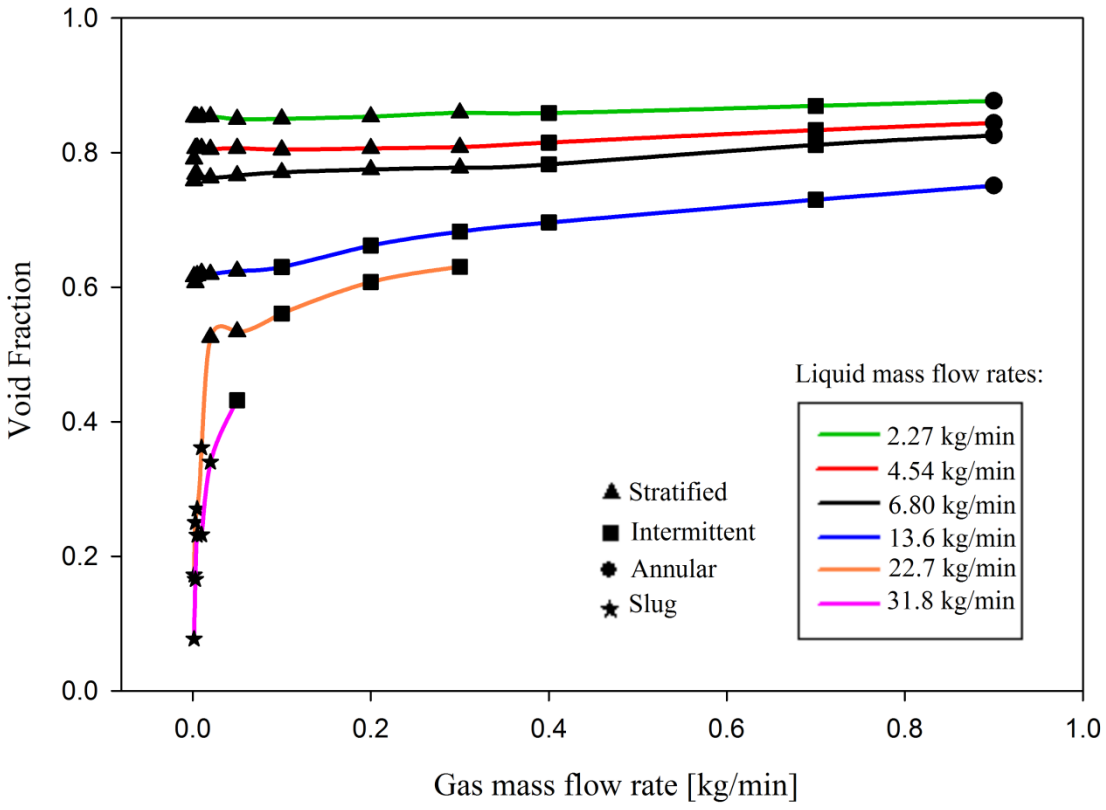

Figure 32 Variation of void fraction with flow pattern -10^{o}

Table 4 Range of void fraction for distinct flow patterns observed in present study for -10^{o}

Flow pattern	**Range of void fraction**
Slug	0.08 - 0.40
Stratified	0.53 - 0.87
Intermittent	0.53 - 0.89
Annular	0.77 - 0.92

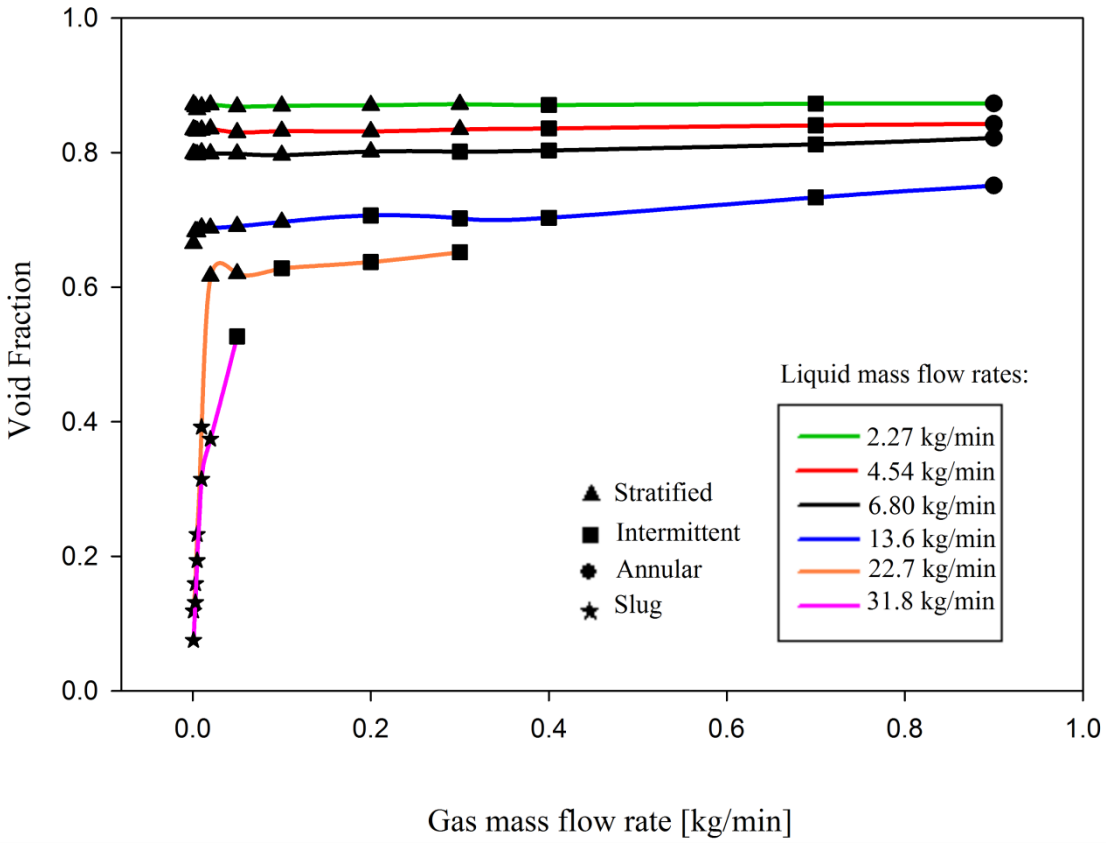

Figure 33 Variation of void fraction with flow pattern -20°

Table 5 Range of void fraction for distinct flow patterns observed in present study for -20°

Flow pattern	**Range of void fraction**
Slug	0.08 - 0.40
Stratified	0.62 - 0.87
Intermittent	0.53 - 0.91
Annular	0.77 - 0.90

4.4.2 PERFORMANCE ANALYSIS OF VOID FRACTION CORRELATIONS FOR DOWNWARD INCLINED PIPE ORIENTATION

A total of 120 void fraction data points were measured in the present study for downward flow orientations. These data points were used to evaluate the performance of thirteen selected correlations from the literature. A comprehensive analysis was performed to suggest the best correlation for the case of downward inclinations. As stated by Godbole et al. (2011), the statistical parameter adopted for correlation performance comparison, is based on discretion of investigator due to ease of calculation and analyses. Different statistical parameters exist in the literature which includes logarithmic ratios, fractional deviation, relative performance factor and many more. Dukler et al. (1964) carried out the first void fraction correlation comparison for horizontal pipe orientation with different pipe diameters and the parameter employed for correlation analysis were standard deviation and arithmetic mean deviation. Palmer (1975) conducted experiments on 51 mm diameter pipe for upward (+4.2^o, +7.1^o and +7.5^o) and downward (-3.8^o, -4.3^o,-6.3^o), percentage error and standard deviation were the parameters used for comparison. Recently Oyewole (2013) conducted inclined experiments for upward and downward flows in 12.7 mm diameter pipe, utilizing the root mean square method and percentage errors as tools for comparison. In the present study, the comparison parameter which was adopted has been used by previous investigators in the same research group, giving excellent results for the evaluation of correlations. The individual correlation performance was established by utilizing the percentage error and root mean square error expressed as:

$$RMS\ error = \sqrt{\frac{1}{N-1}\sum_{i=1}^{N}\left[\frac{(\alpha_{calc})_i - (\alpha_{meas})_i}{(\alpha_{calc})_i}\right]^2}\ x100\%$$

In this section an analysis of the total data set was conducted to determine the best performance correlation. Also, the void fraction data was divided into three regions of $0 < \alpha \leq 0.25$, $0.25 < \alpha \leq$

0.75, $0.75 < \alpha \leq 1$. These ranges were based on flow patterns, the low void fraction range is related to slug flow patterns, and the mid-range is associated with slug, stratified, intermittent and annular, while the high void fraction range is more related to intermittent and annular. Discretizing the entire range of void fraction provides a better interpretation of the analysis, since void correlation performed better at specific regions.

In order to study the pipe diameter effect on the performance of void fraction correlations, a comparison analysis was done with a similar study conducted by Oyewole (2013) on void fraction correlations for 12.7 mm diameter pipe. Thus, the same selection criteria followed by Oyewole (2013) was used in this paper. These criteria are given below:

1. Flow pattern and pipe orientation independent correlations: Different flow patterns and combination of two or more flow patterns were observed in present study. Flow pattern dependent correlation would ultimately fail in predicting void fraction in the transition flow pattern regions because of change in two phase structure in pipe cross section. Also pipe orientation independent correlation would ensure continuity in use of correlation for analyses of all three pipe orientations in present study.

2. Drift flux model correlations: As reported in the literature, drift flux model based void fraction correlations are the top performing correlations due to their ability to predict most accurately the flow physics of two phase flow. Woldesemayat & Ghajar (2007) conducted comparison of void fraction correlations for horizontal and upward inclined pipes. 68 correlations were selected for comparison and 6 correlations performed best, 5 out of the 6 correlations were based on drift flux model. They also conducted void fraction correlations comparison for vertical upward flow, 52 void fraction correlations were analyzed and only 8 correlations performed satisfactorily, all of which are drift flux models.

3. Empirical correlations: Some empirical correlations have been reported in the literature to perform satisfactorily for horizontal and near horizontal pipe orientations e.g., Guzhov et al. (1967)

4. Separated flow model or slip ratio correlations: Separated flows were observed in present study (stratified and annular flows) and some correlations have been reported to perform better than other correlations in the separated region. Bhagwat & Ghajar (2013) conducted correlation comparison for 4227 air-water data points and reported a few top performing separated flow model correlations. Woldesemayat & Ghajar (2007) also reported the top performing correlations in horizontal and upward inclined pipes.

Based on the above mentioned criteria, thirteen correlations were carefully chosen for performance evaluation against experimental data obtained in present study.

1. Bhagwat and Ghajar (2013)
2. Bonnecaze et al. (1971)
3. Cioncoloni and Thome (2012)
4. Gomez et al. (2000)
5. Guzhov et al. (1967)
6. Lockhart and Martinelli (1949)
7. Morooka et al. (1989)
8. Nicklin et al. (1962)
9. Rouhani and Axelsson (1970)
10. Smith (1969)
11. Sun et al. (1981)
12. Woldesemayat and Ghajar (2007)
13. Yashar et al. (2001)

Author/Source	Void Fraction Correlation
	$Drift\ flux\ model: \alpha = \frac{U_{sg}}{C_o(U_{sg} + U_{sl}) + U_{gm}}$
1. Bhagwat and Ghajar (2013)[D]	$C_o = \frac{2 - \left(\rho_g/\rho_l\right)^2}{1 + \left(Re_{tp}/1000\right)^2} + \frac{\left[\sqrt{\left(1 + \left(\rho_g/\rho_l\right)^2 cos\theta\right)/(1 + cos\theta)}\right]^{2/5}}{1 + \left(Re_{tp}/1000\right)^2} + C_{o,1}$ $C_{o,1} = \left(C_1 - C_1\sqrt{\rho_g/\rho_l}\right)\left((2.6 - \beta)) - \sqrt{f_{tp}}\right)(1 - x)^{1.5}$ $U_{gm} = (0.35sin\theta + 0.45cos\theta)\sqrt{\frac{gD_h(\rho_l - \rho_g)}{\rho_l}}(1 - \alpha)^{0.5}C_2C_3C_4$ $C_1 = 0.2, C_2 = \begin{cases} \left(\frac{0.434}{log_{10}\left(\mu_l/0.001\right)}\right)^{0.15} & \left(\mu_l/0.001\right) > 10 \\ 1 & \left(\mu_l/0.001\right) \le 10 \end{cases}$ $C_3 = \begin{cases} \left(La/0.025\right)^{0.9} & La < 0.025 \\ 1 & La \ge 0.025 \end{cases}, La = \sqrt{\sigma/(g\Delta\rho)}/D_h$ $C_4 = -1\ (0^o > \theta \ge -50^o), Fr_{sg} \le 0.1, otherwise\ C_4 = 1$ $Re_{tp} = \frac{(U_{sl} + U_{sg})\rho_l D_h}{\mu_l}, \beta = \frac{U_{sg}}{U_{sl} + U_{sg}}, \frac{1}{\sqrt{f_{tp}}}$ $= -4.0log_{10}\left(\frac{\varepsilon/D_h}{3.7} + \frac{1.256}{Re_{tp}\sqrt{f_{tp}}}\right)$
2. Bonnecaze et al. (1971)[D]	$\alpha = U_{sg}/\left(1.2U_m + 0.35\sqrt{gD\left(1 - \rho_g/\rho_l\right)}\right)$
3. Cioncoloni and Thome (2012)[B]	$\alpha = hx^n/(1 + (h - 1)x^n)$ $h = -2.129 + 3.129\left(\rho_g/\rho_l\right)^{-0.2186}, n$ $= 0.3487 + 0.6513\left(\rho_g/\rho_l\right)^{0.515}$
4. Gomez el al. (2000)[D]	$U_{gm} = 1.53\left(\frac{g\sigma\Delta\rho}{\rho_l^2}\right)^{0.25}\sqrt{1 - \alpha}sin\theta, C_o = 1.15$

5. Guzhov et al. (1967)	$\alpha = 0.81\beta\left(1 - \exp(-2.2\sqrt{Fr}\right), \beta = \frac{U_{sg}}{U_{sl} + U_{sg}}$ $and\ Fr = \frac{\left(U_{sl} + U_{sg}\right)^2}{gD}$
6. Lockhart and Martinelli (1945)[S]	$\alpha = \left[1 + 0.28(1 - x/x)^{0.64}\left({\rho_g}/{\rho_l}\right)^{0.36}\left({\mu_l}/{\mu_g}\right)^{0.07}\right]^{-1}$
7. Morooka et al. (1989)[D]	$\alpha = {U_{sg}}/{(1.08U_m + 0.45)}$
8. Nicklin et al. (1962)[D]	$\alpha = {U_{sg}}/{\left(1.2U_m + 0.35\sqrt{gD}\right)}$
9. Rouhani and Axelsson (1970)[D]	$C_o = 1 + 0.2(1 - x)\left(\frac{gD{\rho_l}^2}{G^2}\right)^{0.25}, U_{gm} = 1.18\left(g\sigma\frac{\rho_l - \rho_g}{{\rho_l}^2}\right)^{0.25}$
10. Smith (1969)[D]	$\alpha = \left(1 + \frac{\rho_g}{\rho_l}\left(\frac{(1-x)}{x}\right)\left[0.4 + 0.6\left(\frac{{\rho_l}/{\rho_g} + 0.4\left({1}/{x - 1}\right)}{1 + 0.4\left({1}/{x - 1}\right)}\right)^{0.5}\right]\right)^{-1}$
11. Sun et al. (1981)[D]	$C_o = \left[0.82 + 0.18\left(P_{Sys}/P_{cr}\right)\right]^{-1}, U_{gm} = 1.41\left(g\sigma\frac{\rho_l - \rho_g}{{\rho_l}^2}\right)^{0.25}$
12. Woldesemayat and Ghajar (2007)[D]	$C_o = \frac{U_{sg}}{U_{sg} + U_{sl}}\left[1 + \left(\frac{U_{sl}}{U_{sg}}\right)^{(\rho_g/\rho_l)^{0.1}}\right]$ $U_{gm} = 2.9(1.22 + 1.22sin\theta)^{(P_{Sys}/P_{cr})}\left[\frac{gD\sigma(1 + cos\theta)\left(\rho_l - \rho_g\right)}{{\rho_l}^2}\right]^{0.25}$
13. Yashar et al. (2001)[S]	$\alpha = \left[1 + \sqrt{\frac{(1-x)gD{\rho_l}^2}{G^2x^3} + \left(\frac{1-x}{x}\right)^{0.9}\left(\frac{\rho_g}{\rho_l}\right)^{0.5}\left(\frac{\mu_l}{\mu_g}\right)^{0.1}}\right]^{-0.321}$

B = Biochemical kinematics mathematical function, D = Drift flux correlation, S = Slip ratio correlation.

A total of 120 void fraction data points were obtained in the present study. These were divided in 35 for an inclination angle of -5^o. 41 points were obtained for the orientation of -10^o and 44 points for -20^o. Each correlation was evaluated so as to compare the experimental data with the predicted data by each correlation. A scatter plot was developed for each of the correlations selected for this study. These types of plots allow identifying the trends of the predicted data. The ±10% and ±20% error bands on the plot aids to visually identify the range within which

correlation is more accurate in predicting the experimental data. Scatter plots for all thirteen correlations are presented in Figures 34, 35 and 36.

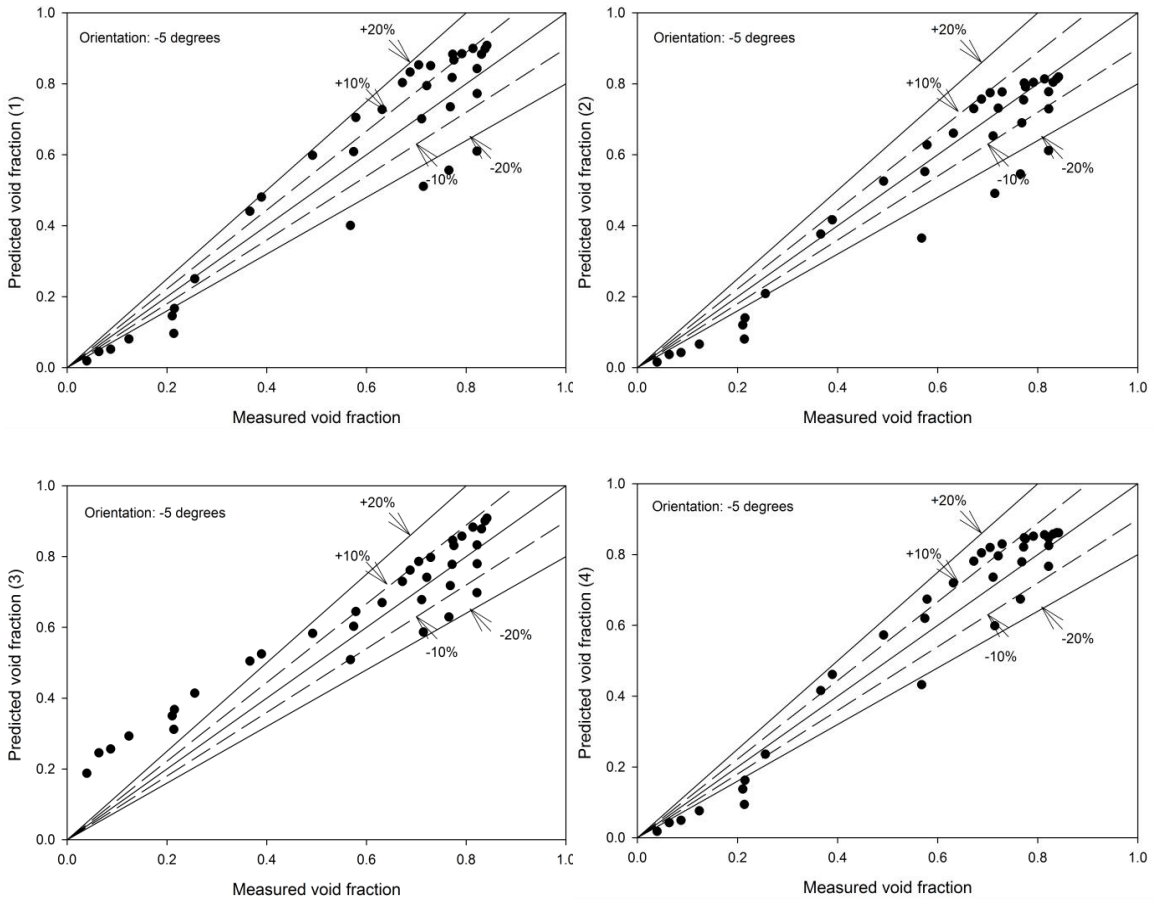

Figure 34 Void fraction data prediction for (1) Bhagwat and Ghajar (2013), (2) Bonnecaze et al. (1971), (3) Cioncoloni and Thome (2012) and Gomez el al. (2000).

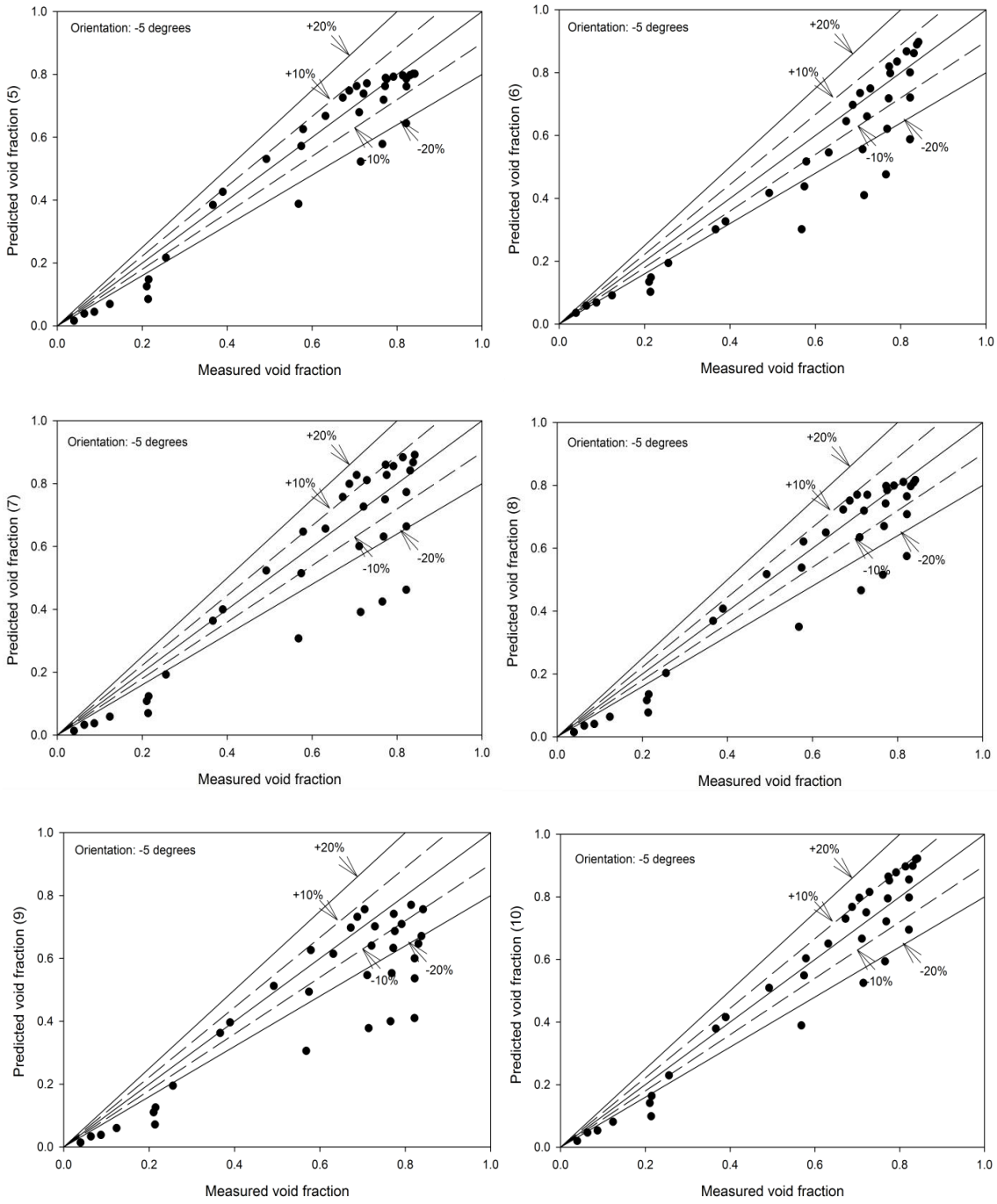

Figure 35 Void fraction data prediction for (5) Guzhov et al. (1967), (6) Lockhart and Martinelli (1945), (7) Morooka et al. (1989), (8) Nicklin et al. (1962), (9) Rouhani and Axelsson (1970), (10) Smith (1969).

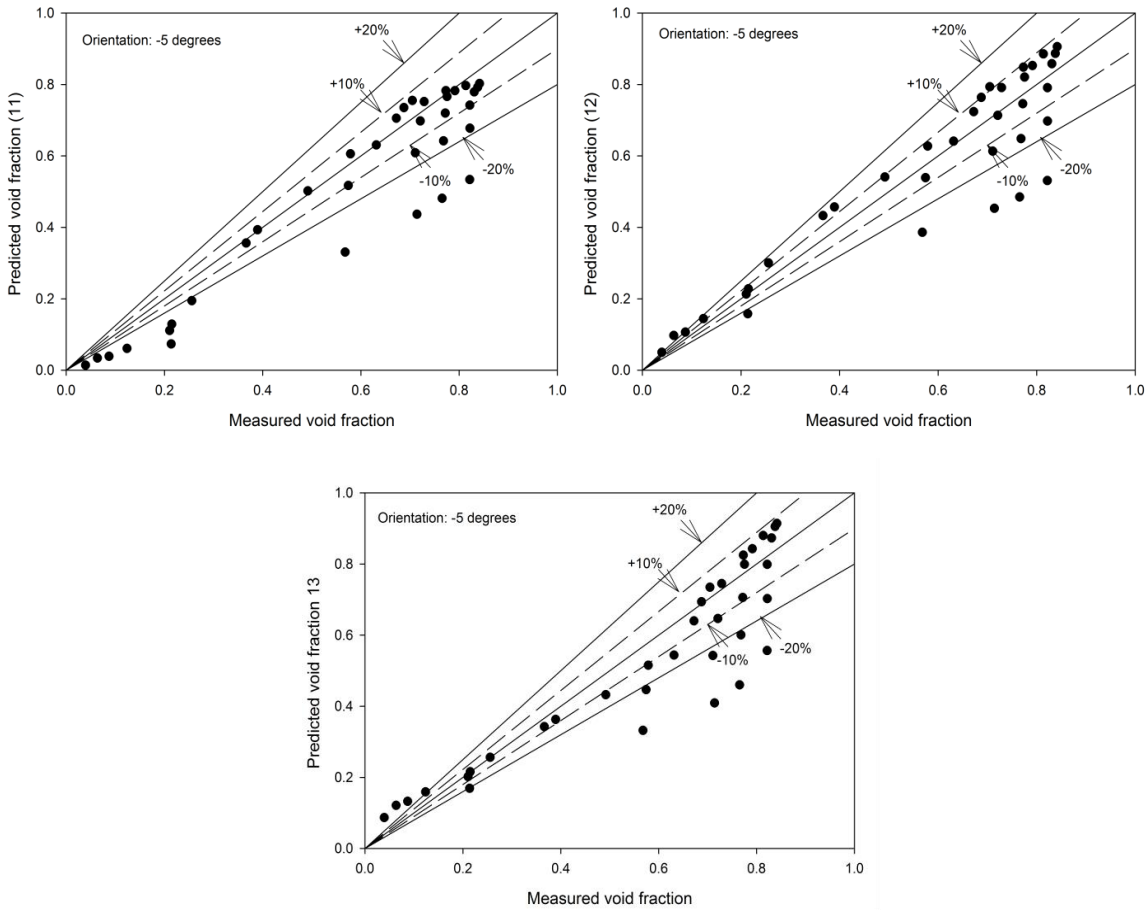

Figure 36 Void fraction data prediction for (11) Sun et al. (1981), (12) Woldesemayat and Ghajar (2007), (13) Yashar et al. (2001).

The scatter plots for -10^{o} and -20^{o} follow similar trends as shown in Figures 34, 35 and 36, therefore it was not relevant to present them. Instead in Tables 6 to 9 a more detailed analysis of the performance of each correlation is offered. In these tables the bolded and underlined values represent the top percentages in terms of accuracy and best performance correlations for each of the void fraction regions and/or error bands.

Table 6 Void fraction correlation comparison for 35 data points for -5°

Pipe Orientation: -5 degrees									
35 Data Points			RMS Error	$0 < \alpha \leq 0.25$ (7 points)		$0.25 < \alpha \leq 0.75$ (15 points)		$0.75 < \alpha \leq 1$ (13 points)	
Correlation	±10% Error	±20% Error	%	±20% Error	±30% Error	±10% Error	±20% Error	±10% Error	±20% Error
1. Bhagwat and Ghajar (2013)	28.6	51.4	9.2	0.0	28.6	20.0	46.7	53.8	84.6
2. Bonnecaze et al. (1971)	57.1	68.6	7.7	0.0	0.0	73.3	86.7	69.2	84.6
3. Cioncolini and Thome (2012)	48.6	**71.4**	9.0	0.0	0.0	40.0	80.0	84.6	100.0
4. Gomez et al. (2000)	42.9	**77.1**	**6.3**	0.0	14.3	20.0	**93.3**	**92.3**	**100.0**
5. Guzhov et al. (1967)	**65.7**	68.6	**6.7**	0.0	14.3	**80.0**	86.7	84.6	84.6
6. Lockhart and Martellini (1949)	45.7	65.7	10.2	28.6	57.1	33.3	66.7	69.2	84.6
7. Morooka et al. (1989)	37.1	65.7	11.8	0.0	0.0	33.3	80.0	61.5	84.6
8. Nickin et al. (1962)	57.1	65.7	8.6	0.0	0.0	73.3	80.0	69.2	84.6
9. Rouhani and Axelsson (1970)	31.4	51.4	14.2	0.0	0.0	60.0	73.3	15.4	53.8
10. Smith (1969)	48.6	**71.4**	**7.0**	0.0	28.6	60.0	86.7	61.5	92.3
11. Sun et al. (1981)	57.1	65.7	9.8	0.0	0.0	73.3	80.0	69.2	84.6
12. Wodelsemayat and Ghajar (2007)	51.4	**77.1**	9.4	**42.9**	**85.7**	46.7	86.7	69.2	84.6
13. Yashar et al. (2001)	51.4	65.7	10.5	28.6	57.1	46.7	73.3	69.2	76.9

Table 7 Void fraction correlation comparison for 41 data points for -10°

Pipe Orientation: -10 degrees									
41 Data Points			RMS Error	$0 < \alpha \leq 0.25$ (6 points)		$0.25 < \alpha \leq 0.75$ (14 points)		$0.75 < \alpha \leq 1$ (21 points)	
Correlation	±10% Error	±20% Error	%	±20% Error	±30% Error	±10% Error	±20% Error	±10% Error	±20% Error
1. Bhagwat and Ghajar (2013)	41.5	61.0	12.1	0.0	0.0	21.4	50.0	66.7	85.7
2. Bonnecaze et al. (1971)	41.5	65.9	13.2	0.0	0.0	42.9	71.4	52.4	81.0
3. Cioncolini and Thome (2012)	**56.1**	**75.6**	**8.8**	0.0	20.0	**57.1**	**85.7**	**71.4**	**90.5**
4. Gomez et al. (2000)	**51.2**	**70.7**	**9.4**	0.0	0.0	21.4	71.4	**85.7**	**90.5**
5. Guzhov et al. (1967)	41.5	68.3	12.2	0.0	0.0	50.0	71.4	47.6	85.7
6. Lockhart and Martellini (1949)	43.9	56.1	15.9	0.0	0.0	35.7	50.0	61.9	76.2
7. Morooka et al. (1989)	36.6	53.7	16.7	0.0	0.0	14.3	50.0	61.9	71.4
8. Nickin et al. (1962)	41.5	65.9	14.2	0.0	0.0	50.0	71.4	47.6	81.0
9. Rouhani and Axelsson (1970)	24.4	41.5	20.3	0.0	0.0	42.9	50.0	19.0	47.6
10. Smith (1969)	53.7	**70.7**	**11.3**	0.0	0.0	42.9	71.4	76.2	90.5
11. Sun et al. (1981)	39.0	53.7	15.6	0.0	0.0	50.0	50.0	42.9	71.4
12. Wodelsemayat and Ghajar (2007)	**53.7**	**73.2**	12.7	**40.0**	**60.0**	42.9	**78.6**	66.7	81.0
13. Yashar et al. (2001)	41.5	56.1	15.7	**40.0**	**60.0**	28.6	50.0	61.9	71.4

Table 8 Void fraction correlation comparison for 44 data points for -20^{o}

Pipe Orientation: -20 degrees									
44 Data Points			RMS Error	$0 < \alpha \leq 0.25$ (6 points)		$0.25 < \alpha \leq 0.75$ (16 points)		$0.75 < \alpha \leq 1$ (22 points)	
Correlation	±10% Error	±20% Error	%	±20% Error	±30% Error	±10% Error	±20% Error	±10% Error	±20% Error
1. Bhagwat and Ghajar (2013)	36.6	**73.2**	12.8	0.0	0.0	18.8	56.3	54.5	95.5
2. Bonnecaze et al. (1971)	56.1	68.3	13.5	0.0	0.0	37.5	50.0	77.3	90.9
3. Cioncolini and Thome (2012)	56.1	68.3	**11.3**	0.0	0.0	**75.0**	**87.5**	50.0	63.6
4. Gomez et al. (2000)	61.0	**75.6**	**10.3**	0.0	0.0	25.0	56.3	**95.5**	**100.0**
5. Guzhov et al. (1967)	**63.4**	**68.3**	**12.6**	0.0	0.0	43.8	50.0	86.4	90.9
6. Lockhart and Martellini (1949)	31.7	43.9	18.1	0.0	0.0	18.8	31.3	45.5	59.1
7. Morooka et al. (1989)	26.8	63.4	17.1	0.0	0.0	12.5	50.0	40.9	81.8
8. Nickin et al. (1962)	51.2	65.9	14.3	0.0	0.0	31.3	50.0	72.7	86.4
9. Rouhani and Axelsson (1970)	24.4	48.8	19.9	0.0	0.0	31.3	50.0	22.7	54.5
10. Smith (1969)	39.0	51.2	14.8	0.0	0.0	25.0	50.0	54.5	59.1
11. Sun et al. (1981)	51.2	65.9	15.5	0.0	0.0	31.3	50.0	72.7	86.4
12. Wodelsemayat and Ghajar (2007)	36.6	58.5	13.5	**50.0**	**83.3**	37.5	50.0	40.9	63.6
13. Yashar et al. (2001)	34.1	46.3	18.0	**83.3**	**100.0**	18.8	31.3	45.5	50.0

Table 9 Void fraction correlation comparison for 120 data points for –downward pipe inclinations

Pipe Orientation:-5, -10, -20 degrees									
120 Data Points			RMS Error	$0 < \alpha \leq 0.25$ (19 points)		$0.25 < \alpha \leq 0.75$ (45 points)		$0.75 < \alpha \leq 1$ (56 points)	
Correlation	±10% Error	±20% Error	%	±20% Error	±30% Error	±10% Error	±20% Error	±10% Error	±20% Error
1. Bhagwat and Ghajar (2013)	35.0	60.8	11.8	0.0	10.5	20.0	51.1	58.9	89.3
2. Bonnecaze et al. (1971)	50.0	65.8	12.1	0.0	0.0	51.1	68.9	66.1	85.7
3. Cioncolini and Thome (2012)	52.5	70.0	**10.1**	0.0	5.3	**57.8**	**84.4**	66.1	82.1
4. Gomez et al. (2000)	50.8	**72.5**	**9.1**	0.0	5.3	22.2	**73.3**	**91.1**	**96.4**
5. Guzhov et al. (1967)	**55.0**	66.7	**11.2**	0.0	5.3	**57.8**	68.9	**71.4**	**87.5**
6. Lockhart and Martellini (1949)	39.2	53.3	15.6	10.5	21.1	28.9	48.9	57.1	71.4
7. Morooka et al. (1989)	32.5	59.2	15.9	0.0	0.0	20.0	60.0	53.6	78.6
8. Nickin et al. (1962)	48.3	64.2	13.0	0.0	0.0	51.1	66.7	62.5	83.9
9. Rouhani and Axelsson (1970)	25.8	45.8	18.9	0.0	0.0	44.4	57.8	19.6	51.8
10. Smith (1969)	45.8	62.5	11.9	0.0	10.5	42.2	68.9	64.3	78.6
11. Sun et al. (1981)	47.5	60.0	14.3	0.0	0.0	51.1	60.0	60.7	80.4
12. Wodelsemayat and Ghajar (2007)	45.8	67.5	12.8	**42.1**	**73.7**	42.2	**71.1**	57.1	75.0
13. Yashar et al. (2001)	40.8	54.2	15.4	**47.4**	**68.4**	31.1	51.1	57.1	64.3

Each table has nine columns ordered as follows: Two columns show the prediction for the entire range of void fraction, one column presents the root mean square error percentage for each correlation, two columns for the range of void fraction between 0 and 0.25 (one for each ±10 and ±20 percentage errors), then two similar columns for the mid-range of void fraction from 0.25 to 0.75, and finally again two columns similarly for the high void fraction range from 0.75 to 1.

PERFORMANCE OF CORRELATIONS FOR VOID FRACTION RANGE ($0 < \alpha \leq 0.25$)

For the low range of void fraction, the overall performance among all the correlations was unsatisfactory. The error bands for this region were selected to be 20% and 30% in order to be able to compare the performance of the correlations. Despite the fact that for the mid and high range of void fraction the percentages of comparison for error bands were 10% and 20% which means better results were obtained in this other regions.

For the case of -5^{o} the highest prediction of void fraction data was observed by Wodelsemayat and Ghajar (2007) with 42.9 % of data points within a ±20% error band, and 85.7 % data points within ±30% error bands. The second highest accuracy percentage was for the case of -5^{o} by two correlations Yashar et al. (2001) and Lockhart and Martellini (1949) with 57.1% of data points within ±30% error bands. Similarly, low performances were registered for inclinations of -10^{o} and -20^{o}. Moreover, for -10^{o} of inclination, the most consistent correlations were Wodelsemayat and Ghajar (2007) and Yashar et al. (2001), with 40% of data points within ±20% error bands and 60% data points for ±30% error bands, for both correlations. For the case of -20^{o}, Yashar et al. (2001) provided the best result which was 100% for 30% error bands and 83.3% for 20% error bands.

PERFORMANCE OF CORRELATIONS FOR VOID FRACTION RANGE ($0.25 < \alpha \leq 0.75$)

Accuracy of correlations improved significantly in this region in comparison with the low void fraction range. For -5^{o}, Gomez et al. (2000) predicted 93.3% of data points within ±20% error

bands. However, Gomez et al. (2000) showed low accuracy for ±10% error bands with only 20% on the points. For this same inclination angle (-5^o), Guzhov et al. (1967) showed much better results in ±10% error bands, predicting 80% of data points.

For -10^o pipe inclination, Cioncolini and Thome (2012) showed the best results, predicting 85.7% of data points for ±20% error bands. The second best was observed to be Wodelsemayat and Ghajar (2007) with 78.6% accuracy in ±20% error bands. It is important to notice that five other correlations performed nearly as good as well, showing predictions of 71.4% for ±20% error bands.

For the case of -20^o of inclination, the efficiency of correlations dropped as observed in the case of low range void fraction. Accuracy seemed to decrease with increasing negative angles of inclination. However, the best results were obtained by Cioncolini and Thome (2012), showing 87.5% of data points in the ±20% error bands. The second best was Gomez et al. (2000) and Bhagwat and Ghajar (2013) with a low 56.3% of accuracy within ±20% error bands.

PERFORMANCE OF CORRELATIONS FOR VOID FRACTION RANGE ($0.75 < \alpha \leq 1$)

For this higher range of void fraction, the overall performance of predictions was better than the previous lower ranges of void fraction. For -5^o of inclination Gomez et al. (2000) was observed to be the best revealing 92.3% of data points within ±10% error bands, also 100% of data points were observed to fall within the ±20% error bands. For this same inclination angle, Smith (1969) showed the second best result with 92.3% and 8 other correlations were 84.6% accurate within ±20% error bands.

For -10^o of inclination Cioncolini and Thome (2012) and Gomez et al. (2000) were the best correlations showing 90.5% accuracy in ±20% error bands. Also, Smith (1969) showed 90.5% of prediction for the ±20% error bands. Other 5 correlations showed good results as well, obtaining 80% of data points within ±20% error bands.

In the case of -20^{o} of inclination, good overall performance was observed at this high range of void fraction. The best correlation was observed to be Gomez et al. (2000) with 95.5 % accuracy for ±10% and 100% of data points within ±20% error bands. Also, Guzhov et al. (1967) and Bhagwat and Ghajar (2013) obtained more than 90% of predictions for 20% error bands.

BEST PERFORMANING CORRELATIONS FOR DOWNWARD INCLINED PIPE ORIENTATION

For -5^{o} pipe orientation, Gomez et al. (2000) performed best with the lowest percent RMS error of 6.3% followed by Guzhov et al. (1967) and Smith (1969) with RMS error of 6.7% and 7% respectively as shown in Table 6.

For -10^{o} pipe orientation, Cioncolini and Thome (2012) perfomed best with a low RMS error of 8.8%, second best was Gomez et al. (2000) with 4% RMS error, followed by Smith (1969) with 11.3% RMS error, these results are shown in Table 7.

Gomez et al. (2000) revealed the best performance with 10.3% RMS error for -20^{o} orientation, followed by Cioncolini and Thome (2012) with 11.3% RMS error and Guzhov et al. (1967) with 10.3% RMS error, as shown in Table 8.

Based on all the downward inclinations studied in the present investigation and the entire range of void fraction, Gomez et al. (2000) with 9.1% RMS error followed by Cioncolini and Thome (2012) with 10.1% RMS error and Guzhov et al. (1967) with a RMS error of 11.2 as shown in Table 9.

EFFECT OF DOWNWARD INCLINATIONS ON PREDICTION OF VOID FRACTION

It was observed that the accuracy of the correlations decreased with higher downward inclination angles, for most of the correlations studied in the present investigation. Gomez et al. (2000) performed very consistently among all the correlations overall. Moreover, Gomez et al. (2000)

also presented a down shift related to the prediction accuracy with increasing downward inclinations. This phenomenon is observed in Figure 37. However, for high void fraction values greater than 0.7, this effect is not observable.

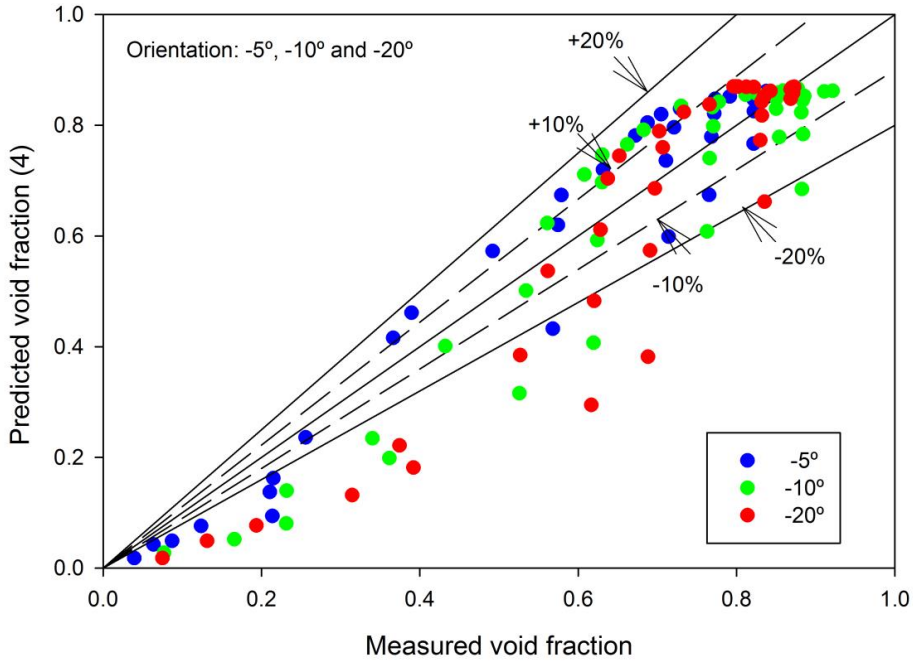

Figure 37 Effect of increasing downward inclinations for void fraction data prediction of Gomez et al. (2000)

In Figure 37 the red dots represent -20°, green -10° and blue -5°. It is noticeable how the performance of the correlation decreases when increasing the downward inclination. The correlation developed by Gomez et al. (2000) tends to under predict the values of void fraction in these cases. However, adjusting some of the parameters in the correlations may eliminate these under predictions. Probably accounting for buoyancy effect, flow pattern factor or gravitational forces would make an improvement on the performance of this correlation.

COMPARISON OF VOID FRACTION CORRELATIONS PERFORMANCE FOR DIFFERENT PIPE DIAMETERS

A study on void fraction was conducted by Oyewole (2013) for a pipe diameter equal to 12.7 mm in the same laboratory where the current investigation took place. As part of the Oklahoma State University two phase flow laboratory team, one of the objectives was to compare both results and evaluate any differences or similarities on the two phase flow with the variation of pipe diameter.

Oyewole (2013) evaluated the performance of thirteen void fraction correlations, as mentioned before the same correlations were studied in the present investigation with the purpose of comparing both results. It can be observed in Table 10 a comparison between the top performance correlations attained by both studies. The top 4 performed correlations for the 12.7 mm diameter pipe study by Oyewole (2013) were: Gomez et al. (2000), Smith (1969), Guzhov et al. (1967) and Bhagwat and Ghajar (2013), four of which were in the top 5 correlations for the present study.

It can be concluded that despite the fact that the pipe diameter was doubled for the case of the present study, the performance of the selected correlations was analogous to the one obtained by Oyewole (2013).

Table 10 Comparison of void fraction correlations performance between 12.7 mm and 25.4 mm pipe diameter

Correlation	**D=12.7 mm Oyewole (2013)**		**D=25.4 mm (present study)**	
	RMS %	**Rank**	**RMS %**	**Rank**
Gomez et al. (2000)	14.70	1	9.13	1
Smith (1969)	14.80	2	11.90	5
Guzhov et al. (1967)	16.60	3	11.15	3
Bhagwat and Ghajar (2013)	17.00	4	11.82	4

CHAPTER V

SUMMARY, CONCLUSIONS AND RECOMMENDATIONS

An experimental setup was designed and constructed, detailed information was provided in preceding chapters. The experimental apparatus was developed for the purpose of two-phase flow pressure drop, void fraction, flow visualization and non-boiling heat transfer measurements for an inclination range of $\pm 20^{o}$. The heat transfer section was reinstalled from a previous experimental setup designed by Tang (2011) and all the instrumentation associated with it was kept the same. Calibration of all the instrumentation associated with the experimental setup (pressure transducer, thermocouples, coriolis flow meters and void fraction section) was performed.

After the experimental setup was constructed, a comprehensive study on flow visualization and void fraction was conducted for near downward pipe orientations. The experiments presented in this paper were divided into two sections: the first was flow patterns and flow mapping and the second was on void fraction.

Flow pattern visualization was performed and four flow patterns were observed: stratified, slug, annular and intermittent flows. Four flow pattern maps were developed per each inclination (0^o, -5^o, -10^o and -20^o) and were concentrated in one flow map, in order to be able to compare transition lines for different inclinations in one flow map. Variation in pipe inclination caused transition lines to shift. Moreover, the developed flow map was compared to the flow map created by Ghajar & Bhagwat (2014), for a similar type of investigation in a smaller pipe diameter. It was observed that transition lines shifted when comparing both.

Void fraction measurement were conducted in three different inclinations (-5^o, -10^o and -20^o). Experiments were performed using air and water as the working fluids in a 25.4 mm diameter pipe and 120 void fraction data points were measured.

Measured void fraction was validated with the prediction of the top performing correlations in the present study as well as with data from other sources. Void fraction correlation comparisons were conducted in order to evaluate their performance for downward near horizontal pipe inclinations and within specific ranges of void fraction. The conclusion and recommendation for the three sections are presented below.

5.1 CONCLUSIONS OF THE FLOW PATTERNS AND FLOW MAPS

Flow visualization was performed on downward orientations (0^o, -5^o, -10^o and -20^o), four distinctive flow patterns were observed: stratified, slug, intermittent and annular. Four flow pattern maps were developed per each downward inclination and were concentrated in one unified flow map. Comparisons between transition lines for different inclinations were analyzed. The transition line from stratified region to slug flow shifted up for the case of downward flow in comparison to the horizontal flow. Barnea (1987) explained that the liquid phase in downward flows is accelerated by the gravitational force acting in the direction of the flow, and since the

fluid is moving faster, then more amount of fluid exits the pipe causing the film thickness to be reduced. This is the reason why these transition lines shifted up for the case of stratified flow.

Also, transition lines from stratified to slug for downward orientations are almost identical. However, there is a small shift up of these transition lines when the inclination angle is increased towards the negative values. For the case of transition lines from stratified to intermittent flow, they shifted from left to right when increasing the gas flow rates and keeping constant liquid flow rates. These were observed to be ordered from left to right in the following order: -5^{o}, -10^{o}, -20^{o}.

The developed flow map was compared to the flow map created by Ghajar & Bhagwat (2014) for a similar type of investigation in a 12.7 mm pipe diameter. By comparing these two flow maps with different pipe diameters, the pipe diameter effect was accounted in the investigation. The first difference that can be observed was that the 25.4 mm flow map has expanded in the gas and liquid flow rates axes in comparison to the 12.7 mm by Ghajar & Bhagwat (2014). Also, the stratified flow regime on the 25.4 mm flow pattern map has a larger area, because of a larger volume of liquid that needed to fill up the pipe, thus stratifications were the predominating flow pattern in the present study's flow map.

Moreover, the bubbly flow pattern was not observed in the present study, in contrary to what was observed by Ghajar & Bhagwat (2014) in a similar type of study in a12.7 mm pipe diameter. Two possible reasons were presented: the first is that the liquid flow rates may not be sufficient to fill the pipe therefore higher liquid flow rates are needed and stratified flows are more common. The second reason may be that due to buoyancy forces the gas bubbles find space at the inner top of the pipe where they colloid and form new and bigger bubbles that will ultimately become plugs or slugs, instead of spherical bubbles flowing with the flow stream.

5.2 CONCLUSIONS OF THE VOID FRACTION MEASUREMENTS AND ANALYSIS

Void fraction measurement were conducted in three different inclinations (-5^o, -10^o and -20^o). Experiments were performed using air and water as the working fluids in a 25.4 mm diameter pipe and 120 void fraction data points were measured. Maximum uncertainty of ±3.9% was calculated for the inclination angle of -5^o for the low range of void fraction of 0.04, however lower uncertainty values were obtained at the high range of void fraction for all inclinations which was approximately ±0.15%. Variation of void fraction with flow patterns was obtained at different pipe inclinations. The range of void fraction for individual flow patterns was identified as well, theses ranges were observed to increase or decrease depending on the pipe inclination. It was observed that at low liquid flow rates the void fraction values remain almost constant and vary from values of void fraction of 0.84 – 0.87. It is important to notice that at high gas flow rates, the void fraction values flatten out and remained almost constant.

Validation of void fraction measurement was performed by comparing with the top best performing correlation of the present study. The selected correlations predicted data within ±15% or less for all three downward pipe inclinations. Also, the validation was done by comparing with inclined void fraction data from Beggs (1972) and Mukherjee (1979) for downward pipe inclinations.

The evaluation performance of thirteen correlations was done in order to obtain the best performing correlation for downward pipe inclinations near horizontal inclinations. The evaluation was performed based on the least RMS error and the most effective correlation in the present study was Gomez et al. (2000). Moreover, a comparison analysis was completed with a similar type of study conducted by Oyewole (2013) in a 12.7 mm diameter pipe for same downward inclinations as in the present study. This was done with the purpose of studying the influence of the pipe diameter in the prediction performance of the correlations. It was observed that Gomez et al. (2000) was the best performing correlation for both studies. Additionaly, it was found that out of the top five correlations in the present study, four correlations: Gomez et al.

(2000), Smith (1969), Guzhov et al. (1967) and Bhagwat and Ghajar (2013) were also best performing correlations for Oyewole (2013).

5.3 RECOMMENDED VOID FRACTION CORRELATIONS

Based on the analysis of the void fraction correlations performance, the following void fraction correlations are recommended for near horizontal downward inclined pipe orientations. These recommendations are restricted to the range of void fraction, $0 < \alpha \leq 0.25$, $0.25 < \alpha \leq 0.75$, $0.75 < \alpha \leq 1$ regions. Refer to Table 11 for recommendations.

Table 11 Recommendation of the best performing correlation for specific void fraction regions for near horizontal downward inclined pipes

Void Fraction Region	**Correlation**
0 - 0.25	Wodelsemayat and Ghajar (2007) / Yashar et al. (2001)
0.25 - 0.75	Cioncolini and Thome (2012)
0.75 - 1	Gomez et al. (2000)

5.4 RECOMMENDATIONS

The experimental setup designed in the present study is capable of measuring heat transfer, pressure drop and void fraction for two phase flow upward and downward near horizontal pipe orientations. The present study was focused on the evaluation of void fraction correlations for downward flow. However, further studies should be conducted on void fraction for upward flows in 25.4 mm pipe diameter. Additionally, heat transfer and pressure drop experiments should be conducted as well. Moreover, further investigations on void fraction, heat transfer and pressure drop could lead to the improvement and develop of new correlations.

REFERENCES

Barnea, A., Shoham, O., & Taitel, Y. (1982). Flow Pattern Transition for Downward Inclined 2 Phase Flow - Horizontal to Vertical. *Chemical Engineering Science, 37*(5), 735-740.

Barnea, A., Shoham, O., & Taitel, Y. (1985). Gas-Liquid Flow in Inclined Tubes: Flow Pattern Transition for Upward Flow. *Chemical Engineering Science, 40*(1), 131-136.

Barnea, D. (1987). A Unified Model for Predicting Flow-Pattern Transitions for the Whole Range of Pipe Inclinations. *International Journal of Multiphase Flow, 13(1),* 1 – 12.

Beggs, H. D. (1972). *An Experimental Study of Two Phase Flow in Inclined Pipes* (PhD), The University of Tulsa, Tulsa, Oklahoma.

Beggs, H.D., & Brill, J.P. (1973). A Study of Two-Phase Flow in Inclined Pipes. *Journal of Petroleum Technology, 25(5)*, 607–617.

Bhagwat, S., & Ghajar, A.J. (2014). A Flow Pattern Independent Drift Flux Model Based Void Fraction Correlation for a Wide Range of Gas-Liquid Two Phase Flow. *International Journal of Multiphase Flow, 59,* 186-205.

Bonnecaze, R.H., Erskine, W., & Greskovic, E.J. (1971). Holdup and Pressure Drop for Two Phase Slug Flow in Inclined Pipes. *AIChE Journal , 17,* 1109-1113.

Cioncoloni, A., & Thome, J.R. (2012). Void Fraction Prediction in Annular Two Phase Flow. *International Journal of Multiphase Flow , 43,* 72–84.

Cook, W. (2008). *An Experimental Apparatus for Measuremet of Pressure Drop and Void Fraction and Non-Boiling Two Phase Heat Transfer and Flow Visulization in Pipes for all Inclinations* (MS), Oklahoma State University, Stillwater.

Dezhang, L., & Ning, O. (1992). Flow Pattern and Heat Transfer behavior of Boiling Two Phase Flow in Inclined Pipes. *Journal of Thermal Science, 1,* 3-6.

Dix, G.E. (1971). *Vapor Void Fractions for Forced Convection with Subcooled Boiling at Low Flow Rates.* (PhD), University of California, Berkeley

Dukler, A.E., Wicks III, M., & Cleveland, R.G. (1964). Frictional Pressure Drop in Two Phase Flow: A Comparison of Existing Correlations for Pressure Loss and Holdup. *AIChE J. , 10,* 38-43.

Ghajar, A. J, & Bhagwat, S. M. (2014). *Non-Boiling Gas-Liquid Two Phase Flow Phenomenon in Near Horizontal Upward and Downward Inclined Pipe Orientations*. World Academy of Science, Engineering and Technology, I*nternational Journal of Mechanical, Aerospace, Industrial and Mechatronics Engineering, 8(6),*1039-1053

Ghajar, A. J. & Tang, C. C. (2007). Heat transfer measurements, flow pattern maps, and flow visualization for non-boiling two-phase flowin horizontal and slightly inclined pipe. *Heat Transfer Engineering, 28*(6), 525-540.

Godbole, P. V., Tang, C. C., & Ghajar, A. J. (2011). Comparison of Void Fraction Correlations for Different Flow Patterns in Upward Vertical Two-Phase Flow. *Heat Transfer Engineering, 32*(10), 843-860.

Gomez, L.E., Shoham, O. , & Taitel, Y. (2000). Prediction of Slug Holdup: Horizontal and Upward vertical. *International Journal of Multiphase flow., 26*, 517-521.

Guzhov, A.L., Mamayev, V.A., & Odishariya, G.E. (1967). *A Study of Transportation in Gas Liquid Systems.* Paper presented at the In: 10th International Gas Union Conference, Hamburg, Germany.

Haramathy, T. Z. (1960). Velocity of large drops and bubbles in media of infinite or restricted extent. *AIChE, 6*, 281-288.

Hasan, A. R. , & Kabir, C. S. (1988). A study of multiphase flow behavior in vertical wells. *SPE Production Engineering, 3*, 263-272.

Hewitt, G.F., & Wallis, G.B. (1963). Flooding and Associated Phenomenon in Falling Film in a Tube. *AERE-R 4614*.

Kokal, S.L., & Stanislav, J.F. (1989). An Experimental Study of Two Phase Flow in Slightly

Inclined Pipes - II Liquid Holdup and Pressure Drop. *Chemical Engineering Science, 44*, 681–693.

Lockhart, R.W., & Martinelli, R.C. (1949). Proposed Correlation of Data for Isothermal Two Phase, Two Component in Pipes. *Chemical Engineering Progress 45*, 39–48.

Mandhane, J.M., Gregory, G.A., & Aziz, K. (1974). A Flow Pattern Map for Gas--Liquid Flow in Horizontal Pipes *International Journal of Multiphase Flow 4*, 537-553.

Morooka, S., Ishizuka, T., Zuka, M. , & Yoshimura, K. (1989). Experimental Study on Void Fraction in a Simulated BWR Fuel Assembly (Evaluation of Cross-Sectional Averaged Void Fraction) *Nuclear Engineering and Design, 114*, 91-98.

Mukherjee, H. (1979). *An Experimental Study of Inclined Two Phase Flow.* (PhD), University of Tulsa, Tulsa, Oklahoma.

Mukherjee, H. & Brill, J.P. (1985). Empirical Equations to Predict Flow Patterns in Two Phase *Inclined Flow. Int. J. Multiphase Flow, 11*, 3, 299-314.

Nicklin, D, J., Wilkes, J.O. & Davidson, J.F. (1962). Two Phase Flow in Vertical Tubes. *Institute of Chemical Engineers, 40*, 61-68.

Oddie, G., Shi, H., Durlofsky , L.J., Aziz, K., Pfeffer, B., & Holmes, J.A. (2003). Experimental Studies of Two and Three Phase Flows in Large Diameter Inclined Pipes. *International Journal of Multiphase Flow*, 29, 527–558.

Oyewole, A. (2013). *Study of flow patterns and void fraction in inclined two phase flow.* Oklahoma State University, Stillwater, OK.

Palmer, C.M. (1975). *Evaluation of Inclined Two Phase Flow Liquid Holdup Correlations using Experimental Data* (MS), The University of Tulsa, Tulsa, OK.

Rouhani, S.Z., & Axelsson, E. (1970). Calculations of Void Fraction in the Subcooled and Quality Boiling Regions. . *International Journal of Heat and Mass Transfer, 13*, 383-393.

Simmons, J.H. , & Harantty, T.J. (2001). Transition from Stratified to Intermittent Flows in Small Angle Upflows. *International Journal of Multiphase Flow, 27*, 599-616.

Smith, S.L. (1969). Void Fraction in Two Phase Flow: A Correlation Based upon an Equal Velocity Head Model. *Proc. Inst. Mech. Engrs, London*, 184, 647-657.

Spedding, P.L., Ferguson, M.E.G., & Watterson, J.K. (1999). A Study of Two-Phase Co-current Flow in Inclined Pipe. *Dev. Chem. Eng. Mineral Process, 7(1/2)*, 147-177.

Spedding, P.L., & Nguyen, V.T. (1980). Regime Maps for Air Water Two Phase Flow. Chemical Engineering Science. *35*, 779-793.

Spedding, P.L., & Spence, D.R. (1993). Flow Regimes in Two-Phase Gas-Liquid Flow. *International Journal of Multiphase Flow, 19, 2*, 245-280.

Sun, K. R., Duffey, & Peng, C. (1981). Prediction of Two Phase Mixture Level and Hydrodynamically Controlled Dryout under Flow Conditions. *International Journal of Multiphase Flow, 7*, 521–543.

Tang, C. C. (2011). *A Study of heat transfer in non-boiling two-phase gas liquid in pipes for horizontal, slightly inclined, and vertical orientations.* Oklahoma State University, Stillwater, Ok.

Tshuva, M., Barnea, D., & Taitel, Y. (1999). Two Phase Flow in Inclined Parallel Pipes. *Int. J. Multiphase Flow, 25*, 1491-1503.

Wallis, G.B. (1969). *One Dimensional Two Phase Flow*: McGraw-Hill Inc. New York.

Woldesemayat, M. A., & Ghajar, A. J. (2007). Comparison of void fraction correlations for different flow patterns in horizontal and upward inclined pipes. *International Journal of Multiphase Flow, 33*, 347-370.

Yashar, D. A., Wilson, M.K. , Kopke, H.R. , Graham, D.M, Chato, J.C., & Newell, T.A. (2001). Investigation of Refrigerant Void Fraction in Horizontal. *MicroFin Tubes. HVAC&R Research, 7,* 67–82.

Zubar, N., & Findlay, J.A. (1965). Average Volumetric Concentration in Two Phase Flow Systems. *J. Heat Transfer, 87*, 435-468.

VITA

EDGAR IGNACIO LARES BARBOZA

Candidate for the Degree of

Master of Science

Thesis: DESIGN OF AN EXPERIMENTAL SETUP FOR TWO PHASE FLOW STUDIES IN NEAR HORIZONTAL UPWARD AND DOWNWARD PIPE ORIENTATIONS

Major Field: Mechanical Engineering

Biographical: Born in Maracaibo, Venezuela son of Milagros Barboza.

Education:

Completed the requirements for the Master of Science in Mechanical Engineering at Oklahoma State University, Stillwater, Oklahoma in July, 2014.

Completed the requirements for the Bachelor of Science in Mechanical Engineering at La Universidad del Zulia, Maracaibo, Zulia, Venezuela in 2009.

Experience:

Project Engineer leading the installation of a 170 MW Steam Turbine in a Combined Cycle Power Plant project.

Graduate student Teaching Assistant for Heat Transfer and Thermodynamics